Volume 6, No. 1, January - June, 2022.

SCIENCE & DEVELOPMENT

(Online)
ISSN 2821-9007

CBAS
College of Basic and Applied Sciences

A Journal of the College of Basic and Applied Sciences (CBAS), University of Ghana

Science and Development

CBAS
College of Basic and Applied Sciences

ISSN: 2550-3421

ISSN: 2821-9007 (Online)

Cover photo:
https://dasbiogas.com/gallery/

Email for Correspondence:

cbas-sdp@ug.edu.gh

Acknowledgement
This issue of the Science and Development was produced with financial support from the Carnegie Corporation of New York through the University of Ghana Building A New Generation of Academics in Africa (BANGA-Africa) Project.

Printed by Digibooks Ghana Ltd.

Published by
College of Basic and Applied Sciences (CBAS)
University of Ghana

Feasibility of using Biogas digesters as a Palm Oil Mill Effluent (POME) Management Tool in a Developing Country: A Ghanaian Case Study

Emmanuel Essien[1*], Imoro Nimoo Abdulai[1], Isaac Eric Buah[1] and Eunice Dazugo[2]

[1]Department of Agricultural Engineering, University of Ghana, Legon, Ghana
[2]CSIR-Institute of Industrial Research
***Corresponding Author:** ing.essien@gmail.com

ABSTRACT

This study investigates the economic feasibility of using biogas digesters for Palm Oil Mill Effluent (POME) management by artisanal palm oil millers in Ghana. A 20 m^3 and 40 m^3 digesters were piloted in two (2) regions in Ghana and data on parameters such as total cost of an operational system, gas production per day, operation cost, and possible selling price for the biogas and liquid produced taken. These system operating parameters coupled with exchange and interest rates were used to compute the Net Present Value (NPV) and Payback Period (PBP) to examine the profitability (NPV >0) of running the system as a business. The base case scenario showed profitability as the NPV was $ 457,881 for the 20 m^2 and $ 922,062 for the 40 m^3 systems. The PBP of the 20 m^3 and 40 m^3 were 0.08 years and 0.06 years respectively. The systems were still profitable even with ± 5 % variation in all the system operational parameters. The analysis showed the suitability of using this technology for small scale processors in the management of POME to stop environmental degradation. The analysis also shows the sustainability of the technology in a developing country context.

Keywords: Net Present Value (NPV); Palm oil mill effluent (POME); Biogas; Economic feasibility; Profitability analysis: Bio-digester

Introduction

The oil palm value chain is one of the most important commodity value chains in Ghana. In terms of food security, it represents a significant source of the country's fats and oils for the populace (Osei-Amponsah et al., 2012). There is also a plethora of derivative products such as wine, pharmaceutics, clothing, roofing materials and baskets that are available as a result of this value chain (Akhbari et al., 2019). The production and marketing of these derivative commodities along the value chain, makes the oil palm crop one of the most important economic crops in Ghana. As a result of this fact, attempts are being made by both government and non-governmental organizations to grow this industry.

The cumulative effect of these programmes/ interventions is increased production, processing and commerce within the oil palm value chain. The sustainability of these gains is however dependent on the ability of various actors in the value chain to scale their production while minimizing the environmental impact of their activities. Consequently, Non-governmental organisations such as Solidaridad West Africa actively incorporate environmental sustainability measures into all its support to stakeholders. For instance, a significant feature of the Best Management Practices (BMP) training to farmers involves the efficient application of organic and/or inorganic fertilizer to minimize its impact on the environment. Such sustainability measures ensure that farm production is sustainably increased with minimal environmental impact. On the processing side of the oil palm value chain, a significant environmental hazard that needs mitigation is the Palm Oil Mill Effluent (POME). This is a by-product of the processing operation which,

although a valuable resource, becomes an environmental hazard if not properly handled. For every tonne of fresh fruit bunches processed, about 0.7 – 1 m^3 of POME is produced. Thus, a small 2 tonnes/hour mill will produce about 1.4 – 2 m^3 for every hour of operation. This volume multiplied by the usual long hours of operation of the mills brings into sharp focus the scale of the POME problem mills have to deal with.

Most small scale or artisanal millers simply spill the untreated POME unto land. A few mills have trenches that lead to dug-outs where the POME goes to. These dugouts are simply covered with earth when full. These disposal methods cause serious damage to the environment. The continuous draining of the POME unto the bare floor makes the processing centres highly insanitary as the POME mixes with the soil to create a soggy dark bacteria filled soil-POME mix. The part of the POME that seeps into the soil ends up killing soil microorganisms as the POME is released hot (60 - 80° C) and acidic (pH 3.3 – 4.6)(Corley & Tinker, 2003). A significant portion of the POME also drains unto nearby lands making it waterlogged. Mills that are close to water bodies also end up polluting them with POME. This perilous picture of land and water pollution is representative of most artisanal or small-scale mills in Ghana.

Globally, biogas digesters are one of the most prevalent tools for treating POME in the oil palm industry(Tan & Lim, 2019; Tan et al., 2021)the motivation and support from mills still reported low in Malaysia. This paper aims to discuss the benefits and drawbacks of POME utilisation in the palm oil supply chain based on environmental, social and economic concerns to review the favourability of POME elimination. A zero effluent approach is introduced based on POME evaporation technique, undiluted clarification practice and water recycling strategy as an alternative for conventional POME management approaches. An integrated palm oil complex concept is proposed which includes new palm oil processing approach that eliminates POME and provides industrial symbiosis possibilities within palm oil upstream and downstream sectors to promote sustainability of palm oil industry with balanced economic and environmental advantages. A comparative study between POME utilisation (Case 1 and 2. They allow mills to adequately treat POME to reduce the Biological Oxygen Demand (BOD) as anything beyond 5000 mg/l will have deleterious effect on the soil (Rankine & Fairhurst, 1999). The use of biogas digesters also allows the capture and an environmentally safe repurposing (combustible fuel for cookers, electric generators, light bulbs, steamers, etc.) of methane (CH_4) a greenhouse gas which is twenty one (21) times more lethal to the ozone layer than carbon dioxide (CO_2).

The Ghanaian ecosystem is not completely alien to the use of biogas digesters. There is literature reporting several biogas digesters being used for several purposes since the 1960's. The biogas digesters were mostly institutional (treatment of waste for schools, hospitals, abattoirs, etc.), communal and household systems (Bensah & Brew-Hammond, 2010). The main purpose of the biogas digester systems in Ghana has been the generation of biogas for cooking and electricity production and not the treatment of organic waste to address the sanitation issues or the use of the treated waste as organic fertilizer (Ahiataku-Togobo, 2016). This was because biogas was seen as a means of reducing Ghana's reliance on wood fuel which constituted 72 % of the nation's primary energy supply (Arthur et al., 2011). Most of the biogas digesters however failed shortly after the projects that deployed them ended. Several reasons have been adduced for the consistent failure of biogas project across the years. Some are non-availability of organic waste, breakdown of system component, absence of maintenance services, lack of operational knowledge and bad user experience (Bensah & Brew-Hammond, 2010). It is also worth noting that most of the identified causes of the failure have economic underpinnings. This is because there would not be any issues of not being able to replace faulty system components if the system generated enough residual income to replace such components. Such residual income would also allow the managers to afford all required routine maintenance activities, procure alternative organic waste streams if original stream is compromised, organize refresher courses for operators to enhance service delivery and improve user experience.

The underlying economic underpinnings of the causes of failure makes it imperative that one conducts an economic analysis of specific biogas systems to ensure that they are sustainable.

Although the general biogas literature is replete with economic feasibility studies of these systems, those analysis may not be directly applicable to the developing country setting where even institutional systems are relatively small and the nature of organic waste differs (Gebrezgabher et al., 2010; Lok et al., 2020; Meyer et al., 2021; Vo et al., 2018; Zhang & Xu, 2020)management and policy scenarios were investigated. Economic evaluations of all scenarios, except no subsidy scenario, show positive NPV. The highest NPV and IRR values are observed under reverse osmosis (RO. There have been efforts to study the economic feasibility of some biogas projects in Ghana. Kemausuor et al., (2016) studied the socio-economic feasibility of a 300 m^3 biogas system in a rural community in Ghana. The study found a Net Present Value (NPV) of $ 22,000 with a 16 years Payback Period (PBP) at a 10 % discount rate. Their proposed system however only works if there is a subsidy as only 5 % of the surveyed households were willing to pay the estimated base tariff of $ 30/ m^3 for the biogas produced. Mohamed et al. (2017) also investigated the feasibility of integrating a biogas digester into a waste treatment plant in Ghana. The simulations showed a profitable NPV at a discount rate of 23 % and a PBP of 5 years. Cudjoe et al. (2021) net present value, investment payback period, levelized cost of energy, and internal rate of return methods. A sensitivity analysis based on two scenarios (optimistic and pessimistic also modelled the economic feasibility of using biogas from food waste to generate electricity in two large cities (Accra and Kumasi) in Ghana. The study found that the project was only economically feasible when the discount rate did not exceed 20 % in both cities.

The utility of the results of the reported feasibility studies in Ghana are however highly sensitive to the plant and machinery cost, type of waste and the discount rates. It is therefore important that one performs an economic feasibility analysis whenever one intends to use a different type of waste (POME) and machinery as in this study's particular context. This study therefore reports on the economically feasible use of a 20 m^3 and 40 m^3 biogas digester for the treatment of POME in the Eastern and Central regions of Ghana.

Materials and Methods

Two balloon type biogas digesters were constructed at two artisanal mills in Kade (Eastern Region) and Fosu (Central Region). The two sites were chosen so as to capture the predominant technologies used in oil palm processing. This is important as the quality of POME is dependent on processing technology used in the artisanal process thus any economic analysis must take this into account. Aside being in the largest artisanal palm oil processing regions in Ghana, these locations were also chosen because they had all the main technologies and processes prevalent at most artisanal mills. The POME produced there was therefore expected to be representative of the majority of artisanal mills due to the similarities in the processing technologies and operations.

Study Area Description

Mill A (Kade)

The mill at Kade is a tolling centre where farmers bring their Fresh Fruit Bunches (FFB) to be processed for a fee. This mill mostly spills the POME into an uncemented channel that drains the POME into nearby land. A 40 m^3 biogas digester was constructed to hold and treat the POME. The digestate of this system will serve as liquid fertilizer for the numerous oil palm nurseries in the area. At the time of the study, a nursery farmer was willing to buy the digestate at GHS 5 per 25 litre gallon (i.e. $ 0.0425 per litre assuming GHS 1 = $ 0.17).

Mill B (Fosu)

The mill at Fosu was also a tolling site owned and managed by a cooperative of about 15 women. The small nature of their operation allows the processors to carry the POME and dispose it in some bushes behind the mill. These bushes however form part of the bank of a small stream

that flows near the processing center. There is therefore the likelihood of POME being washed into the stream when it rains. This, as amply explained earlier, is bad for the environment. Based on the volume of production, a 20 m^3 biogas digester was set up at this site.

Economic assessment

The economic analysis was conducted using the Discounted Cash flow (DCF) method (Ahmad et al., 2020; Lee et al., 2021; Okolie et al., 2021)the cellulose and hemicellulose fractions of lignocellulosic biomass are catalytically converted to γ-valerolactone (GVL. This involved an analysis of capital cost of the 20 m^3 and 40 m^3 system, respective operation costs and revenue streams from the operation. Economic indicators of profitability such as Net Present Value (NPV) and Payback Period (PBP) were computed.

The cost of the installed biogas digesters (Table 1) were given by the supplier of the system (Webber Energy Ghana) and this cost included the cost of the biogas digesters as well as all civil works necessary for the operationalization of the system.

Table 1: Summary of parameters used for base case economic analysis

Parameter	Unit	Value
Cost of digester (20 m^3)	USD ($)	6600
Biogas flow rate (20 m^3)	m^3/day	2
Cost of digester(40 m^3)	USD ($)	9500
Biogas flow rate (40 m^3)	m^3/day	4
Life span	Years	15
Interest rate	%	0.16[a]
Operating cost of 40 m^3 biogas digester (15 % of capital cost of digester)	*USD/year	1,425
Operating cost of 20 m^3 biogas digester (15 % of capital cost of digester)	USD/year	990
Selling price of 25l of liquid fertilizer	USD	0.85
Exchange rate		GHS 1= $ 0.17
Cost of LPG gas	GHS/l	3.5
	GHS/m^3	3500
	USD/m^3	595
Operating days per year	Days	261
Selling price of biogas (LPG/3)	USD/m^3	160.8108

[a]Bank of Ghana reference rate

The cost of the installed system therefore constituted the first cash outflow item. The second cash outflow item was the operating cost which was a summation of the estimated annual cost of maintenance (5 % of cost of installed system) and the estimated cost of labour to man the system (10 % of cost of installed system). Using the 16 % Bank of Ghana reference rate, the operating cost was discounted over the 15 year life span of the system and used to compute the Net Present Value (NPV) using equation 1.

$$NPV = -C_O + \sum_{t=1}^{n} \frac{C_1}{(1+i)^t} \quad (1)$$

Where

C_O= Cost of installed biogas digester system

C_1= Total operating cost

n = lifespan of biogas digester

t = number of years

i = discount (interest) rate

The Payback Period (PBP) which represents the duration needed for an investment to pay for itself was computed using equation 2

$$Payback\ Period\ (PBP) = \frac{Total\ cost\ of\ installed\ bio-digester\ system}{Annual\ Profits} \quad (2)$$

Sensitivity Analysis

The volatile nature of micro/macro-economic indicators in developing countries makes it imperative to vary some of the parameters used in the economic analysis to better understand how they affect the profitability of the enterprise. The parameters varied during the sensitivity analysis were the discount rates, operating costs, selling price of liquid fertilizer and gas production volumes and selling price of biogas produced. These were varied at ±5 % interval as this was assumed to reasonably model the volatilities in the above mentioned parameters in a developing country. This was used to populate the sensitivity tables (Tables 2, 3, 4 and 5). Tornado charts were also used to study the relative comparative changes in parameters when it comes to NPV and PBP.

Results and Discussions

The economic analysis of the base case parameters (Table 1) showed the 20 m^3 and 40 m^3 biogas digesters to be profitable (NPV > 0). This was evident as an NPV of $ 457,881 and $ 922,062 was found for the 20 m^3 and 40 m^3 biogas digesters respectively over the 15 year lifespan of the system (Tables 2 and 3). This estimated NPV was however specific to operational parameters such as interest rate, system operating cost, selling price of liquid fertilizer, exchange rate, selling price of biogas and the gas production per day stipulated for the base case. The study therefore also investigated the profitability of the system when there is a ±5 % variation in the operational parameters for the 20 m^3 (Table 2) and 40 m^3 (Table 3) biogas digesters. The results also indicated profitability even with the ±5 % variations in the operational parameters of both systems.

Table 2: Summary sensitivity Analysis of Net Present Value (NPV) for 20 m³ biogas digester system

20 m³ biogas digester (NPV)					
Interest Rate ± 5%		Operating Cost ± 5%		Selling price of liquid fertilizer ± 5%	
% Change	**NPV**	**% Change**	**NPV**	**% Change**	**NPV**
-5%	475857	-5%	458157	-5%	457782
0%	457881	0%	457881	0%	457881
5%	441006	5%	457605	5%	457980
Selling price of Biogas ± 5%		Gas production per day ± 5%		Exchange Rate ± 5%	
% Change	**NPV**	**% Change**	**NPV**	**% Change**	**NPV**
-5%	434480	-5%	434480	-5%	434381
0%	457881	0%	457881	0%	457881
5%	481282	5%	481282	5%	481381

Table 3: Summary sensitivity Analysis of Net Present Value (NPV) for 40 m³ biogas digester system

40 m³ biogas digester (NPV)					
Interest Rate ± 5%		Operating Cost ± 5%		Selling price of liquid fertilizer ± 5%	
% Change	**NPV**	**% Change**	**NPV**	**% Change**	**NPV**
-5%	958115	-5%	922459	-5%	921889
0%	922062	0%	922062	0%	922062
5%	888216	5%	921665	5%	922235
Selling price of Biogas ± 5%		Gas production per day ± 5%		Exchange Rate ± 5%	
% Change	**NPV**	**% Change**	**NPV**	**% Change**	**NPV**
-5%	875260	-5%	875260	-5%	875087
0%	922062	0%	922062	0%	922062
5%	968864	5%	968864	5%	969037

The study also used Tornado charts to determine which operational parameters had the most impact on the profitability of the system. This is to enable managers of the system to proportionately focus their effort on the operational parameters for profit maximization. The charts showed that for both 20 m^3 (Figure 1) and 40 m^3 (Figure 2) systems, the most impactful operational parameters (from most to least) where exchange rates, gas production per day, selling price of biogas and the interest rate. Due to the fact that managers of the system have no control over exchange rates, it therefore becomes important that all effort is made to optimize gas production and negotiate better prices for the biogas produced as well as interest rates from their lenders. The selling price of liquid fertilizer and the operational cost were the least impactful when it came to the profitability of the system. The selling price of liquid fertilizer (digestate) from the system was low relative to the other operational parameters because fertilizer (commercial) in general is relatively cheap because of government subsidies. The operational cost was also low because the systems as piloted is mostly automated and requires little human effort.

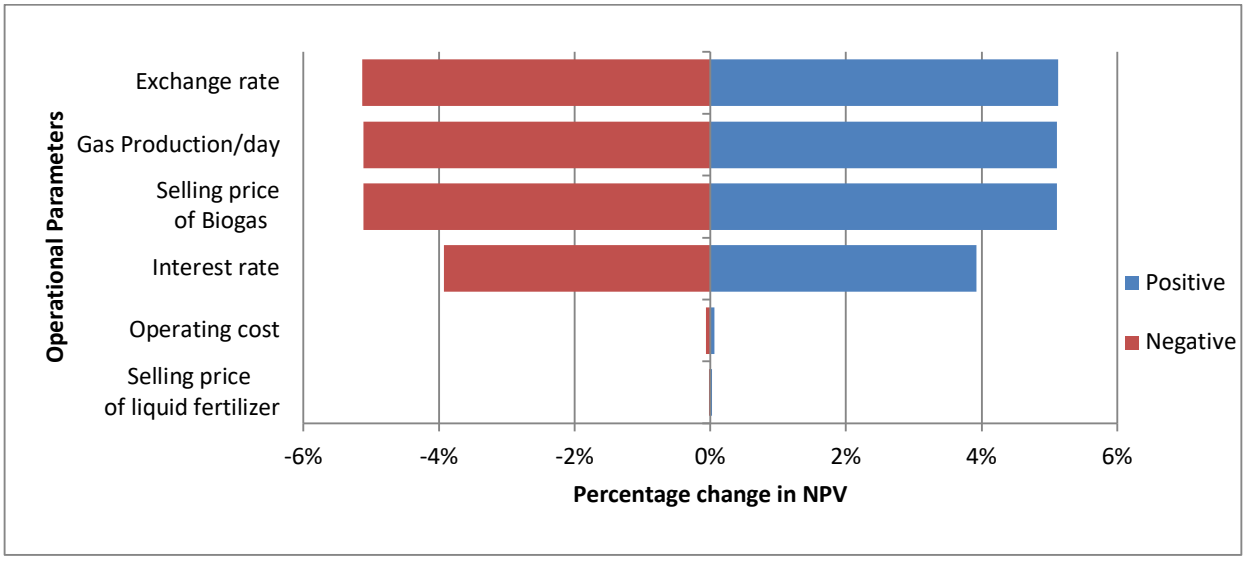

Figure 1: Impact on Net Present Value (NPV) by percentage change in operational parameters for 20 m^3

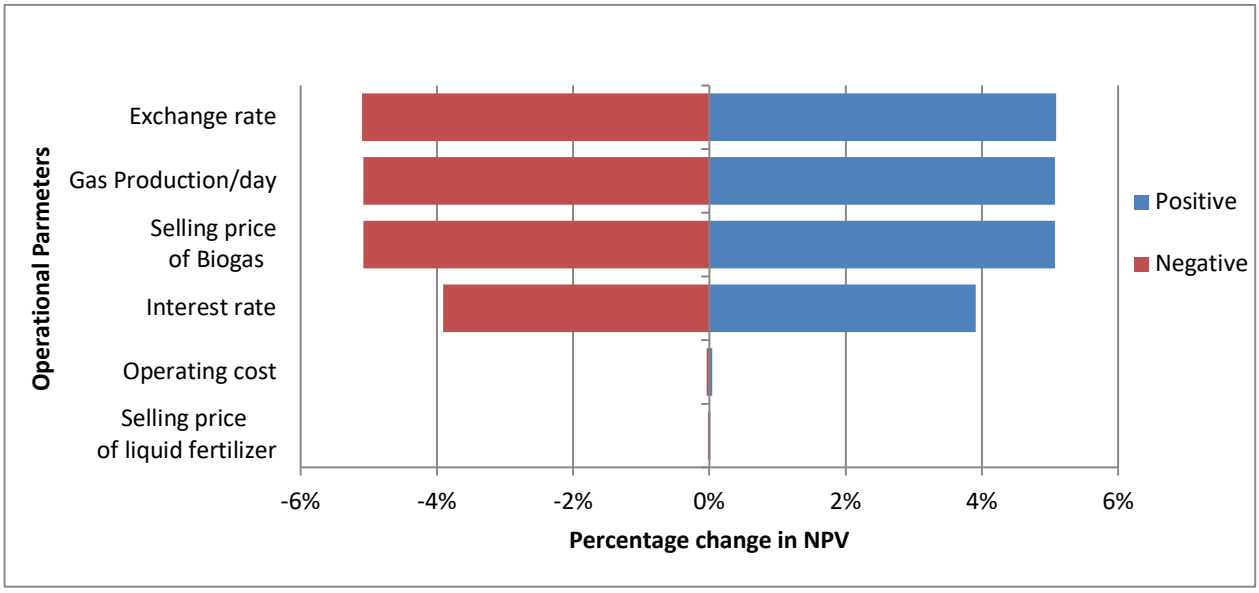

Figure 2: Impact on Net Present Value (NPV) by percentage change in operational parameters for 40 m³

Another critical estimate that was satisfactorily low for both biogas digesters was the Payback Period (PBP). This factor is important because, in developing countries, some renewable energy projects are funded with loans which must be repaid for the sustainability of the fund (Donastorg et al., 2017). The ability of a system to pay for itself quickly ensures that users are able to pay off all loans needed for the system. The PBP for the 20 m³ and 40 m³ in the base case were 0.079 years and 0.057 years respectively. A ± 5 % variation in all the operational parameters only showed marginal deviation from the base case for both the 20 m³ and 40 m³ systems.

Table 4: Summary sensitivity Analysis of Payback Period (PBP) for 20 m³ biogas digester system

20 m³ biogas digester (PBP)					
Interest Rate ± 5%		Operating Cost ± 5%		Selling price of liquid fertilizer ± 5%	
% Change	**PBP**	**% Change**	**PBP**	**% Change**	**PBP**
-5%	0.079223891	-5%	0.079176846	-5%	0.079240772
0%	0.079223891	0%	0.079223891	0%	0.079223891
5%	0.079223891	5%	0.079270992	5%	0.079207017
Selling price of Biogas ± 5%		Gas production per day ± 5%		Exchange Rate ± 5%	
% Change	**PBP**	**% Change**	**PBP**	**% Change**	**PBP**
-5%	0.08342704	-5%	0.08342704	-5%	0.083445761
0%	0.079223891	0%	0.079223891	0%	0.079223891
5%	0.075423947	5%	0.075423947	5%	0.075408652

Table 5: Summary sensitivity Analysis of Payback Period (PBP) for 40 m³ biogas digester system

40 m³ biogas digester (PBP)					
Interest Rate ± 5%		Operating Cost ± 5%		Selling price of liquid fertilizer ± 5%	
% Change	**PBP**	**% Change**	**PBP**	**% Change**	**PBP**
-5%	0.056858082	-5%	0.056833846	-5%	0.056868654
0%	0.056858082	0%	0.056858082	0%	0.056858082
5%	0.056858082	5%	0.056882339	5%	0.056847515
Selling price of Biogas ± 5%		Gas production per day ± 5%		Exchange Rate ± 5%	
% Change	**PBP**	**% Change**	**PBP**	**% Change**	**PBP**
-5%	0.059865771	-5%	0.059865771	-5%	0.059877491
0%	0.056858082	0%	0.056858082	0%	0.056858082
5%	0.054138152	5%	0.054138152	5%	0.054128571

The effect of the various operational parameters on the PBP was also investigated using Tornado charts (Figure 3 and 4). The exchange rate, selling price of biogas and gas production per day were the most impactful parameters with respect to the PBP. This is consistent with what was found with respect to the NPV as regards the effect of the respective operational parameters.

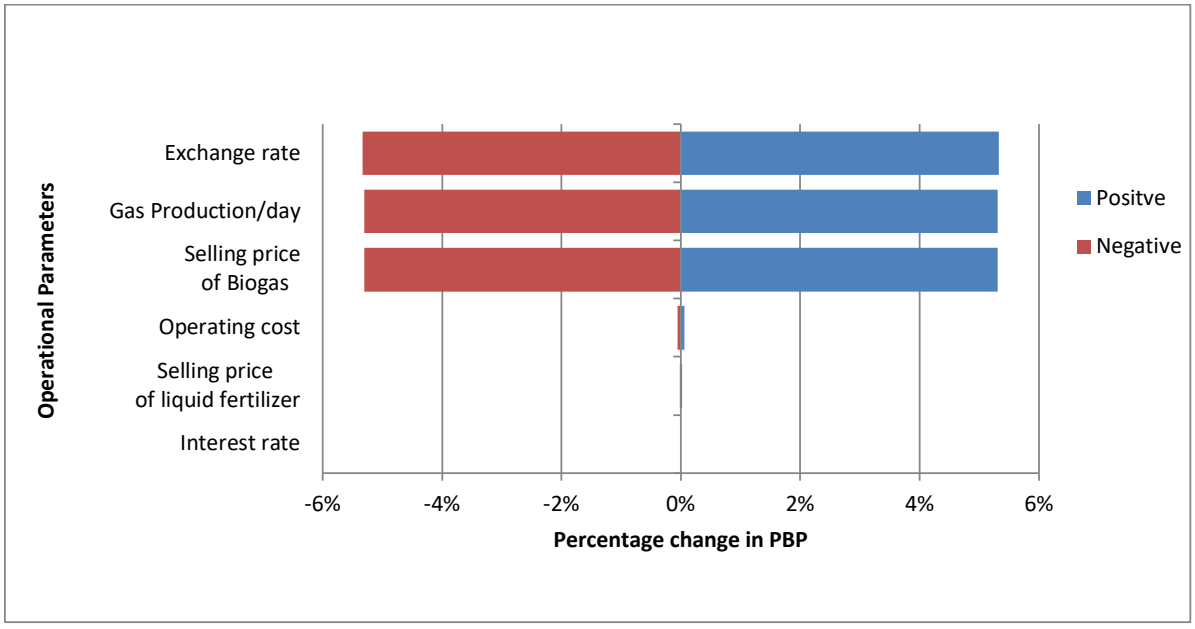

Figure 3: Impact on Payback Period (PBP) by percentage change in base operational parameters for 20 m³

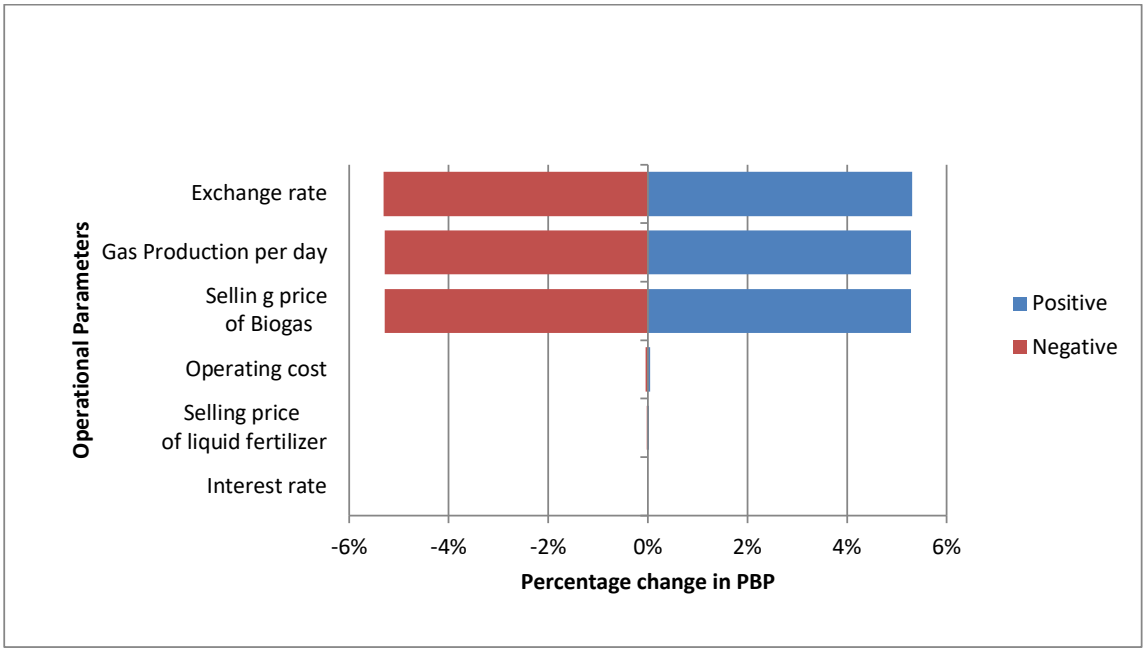

Figure 4: Impact on Payback Period (PBP) by percentage change in operational parameters for 40 m³

As seen in the Table 1, the capital cost for such renewal energy project may be beyond the ability of the artisanal palm oil processors. The profitability illustrated in this study could be used to convince commercial banks to provide funding for such projects. The most impactful operational parameters found in this study could also be used as key performance indicators by relevant parties to ensure that the system and its managers remain efficient at all times.

In addition to other works on economic feasibility of biogas digesters in a developing country context ((Kemausuor et al., 2016; Mohamed et al., 2017), this work also confirms that biogas projects are an economically viable alternative to waste management and treatment. This confirmation is necessary as both works considered biogas capacities (300 m^3 and 9000 m^3) which are impractical for most oil palm processors due to the cost implications. The sizes of these larger systems also introduced other parameters such as skilled labour requirements which are not relevant for small scale users. This work therefore covers the scenario which is relevant for small scale palm oil processors and other small scale food processors and the economic viability of using biogas plants for waste treatment.

Conclusion

The study found the 20 m^3 and 40 m^3 biogas digester systems to be profitable judging from the NPV and PBP values from the base case and the sensitivity analysis. The factors most impactful of the profitability of the system analyzed were exchange rate, selling price of biogas and gas production per day as seem in the tornado charts. It is therefore imperative that managers of the system work hard to continuously improve the gas production volumes as well as negotiate better prices for the biogas produced. Although the liquid fertilizer produced by the system was the least impactful due to its relatively low cost, better marketing could allow the managers to get better pricing from its use. A lean and efficient operation would also enable managers significantly cut down on operations cost therefore boosting the profitability of the system.

Funding Support

The author wishes to acknowledge Solidaridad West Africa for providing the funding for this work.

References

Ahiataku-Togobo, W. (2016). *BIOGAS TECHNOLOGY-WHAT WORKS FOR GHANA?* 25.

Ahmad, N., Ahmad, N., & Ahmed, U. (2020). Process design and techno-economic evaluation for the production of platform chemical for hydrocarbon fuels from lignocellulosic biomass using biomass-derived γ-valerolactone. *Renewable Energy*, *161*, 750–755. https://doi.org/10.1016/j.renene.2020.07.028

Akhbari, A., Kutty, P. K., Chuen, O. C., & Ibrahim, S. (2019). A study of palm oil mill processing and environmental assessment of palm oil mill effluent treatment. *Environmental Engineering Research*, *25*(2), 212–221. https://doi.org/10.4491/eer.2018.452

Arthur, R., Baidoo, M. F., & Antwi, E. (2011). Biogas as a potential renewable energy source: A Ghanaian case study. *Renewable Energy*, *36*(5), 1510–1516. https://doi.org/10.1016/j.renene.2010.11.012

Bensah, E. C., & Brew-Hammond, A. (2010). *Biogas technology dissemination in Ghana: History, current status, future prospects, and policy significance*. *1*(2), 18.

Corley, R. H. V., & Tinker, P. B. (2003). *The Oil Palm* (Fourth Edition). Blackwell Science.

Cudjoe, D., Nketiah, E., Obuobi, B., Adu-Gyamfi, G., Adjei, M., & Zhu, B. (2021). Forecasting the potential and economic feasibility of power generation using biogas from food waste in Ghana: Evidence from Accra and Kumasi. *Energy*, *226*, 120342. https://doi.org/10.1016/j.energy.2021.120342

Donastorg, A., Renukappa, S., & Suresh, S. (2017). Financing Renewable Energy Projects in Developing Countries: A Critical Review. *2nd International Conference on Green Energy Technology (ICGET 2017)*. https://doi.org/doi:10.1088/1755-1315/83/1/012012

Gebrezgabher, S. A., Meuwissen, M. P. M., Prins, B. A. M., & Lansink, A. G. J. M. O. (2010). Economic analysis of anaerobic digestion—A case of Green power biogas plant in The Netherlands. *NJAS - Wageningen Journal of Life Sciences*, *57*(2), 109–115. https://doi.org/10.1016/j.njas.2009.07.006

Kemausuor, F., Bolwig, S., & Miller, S. (2016). Modelling the socio-economic impacts of modern bioenergy in rural communities in Ghana. *Sustainable Energy Technologies and Assessments*, *14*, 9–20. https://doi.org/10.1016/j.seta.2016.01.007

Lee, B., Lim, D., Lee, H., Byun, M., & Lim, H. (2021). Techno-economic analysis of H2 energy storage system based on renewable energy certificate. *Renewable Energy*, *167*, 91–98. https://doi.org/10.1016/j.renene.2020.11.049

Lok, X., Chan, Y. J., & Foo, D. C. Y. (2020). Simulation and optimisation of full-scale palm oil mill effluent (POME) treatment plant with biogas production. *Journal of Water Process Engineering*, *38*, 101558. https://doi.org/10.1016/j.jwpe.2020.101558

Meyer, E. L., Overen, O. K., Obileke, K., Botha, J. J., Anderson, J. J., Koatla, T. A. B., Thubela, T., Khamkham, T. I., & Ngqeleni, V. D. (2021). Financial and economic feasibility of bio-digesters for rural residential demand-side management and sustainable development. *Energy Reports*, *7*, 1728–1741. https://doi.org/10.1016/j.egyr.2021.03.013

Mohamed, M., Egyir, I. S., Donkor, A. K., Amoah, P., & Nyarko, S. (2017). Feasibility study for biogas integration into waste treatment plants in Ghana. *Egyptian Journal of Petroleum*, *26*(3), 695–703. https://doi.org/10.1016/j.ejpe.2016.10.004

Okolie, J. A., Nanda, S., Dalai, A. K., & Kozinski, J. A. (2021). Techno-economic evaluation and sensitivity analysis of a conceptual design for supercritical water gasification of soybean straw

to produce hydrogen. *Bioresource Technology*, *331*, 125005. https://doi.org/10.1016/j.biortech.2021.125005

Osei-Amponsah, C., Visser, L., Adjei-Nsiah, S., Struik, P. C., Sakyi-Dawson, O., & Stomph, T. J. (2012). Processing practices of small-scale palm oil producers in the Kwaebibirem District, Ghana: A diagnostic study. *NJAS - Wageningen Journal of Life Sciences*, *60–63*, 49–56. https://doi.org/10.1016/j.njas.2012.06.006

Rankine, I. R., & Fairhurst, T. H. (1999). *Oil Palm Field Handbook* (Vol. 2). Potash and Phosphate Institute.

Tan, Y. D., & Lim, J. S. (2019). Feasibility of palm oil mill effluent elimination towards sustainable Malaysian palm oil industry. *Renewable and Sustainable Energy Reviews*, *111*, 507–522. https://doi.org/10.1016/j.rser.2019.05.043

Tan, Y. Y., Bello, M. M., & Abdul Raman, A. A. (2021). Towards cleaner production in palm oil industry: Advanced treatment of biologically-treated POME using palm kernel shell-based adsorbent. *Cleaner Engineering and Technology*, *2*, 100079. https://doi.org/10.1016/j.clet.2021.100079

Vo, T. T. Q., Wall, D. M., Ring, D., Rajendran, K., & Murphy, J. D. (2018). Techno-economic analysis of biogas upgrading via amine scrubber, carbon capture and ex-situ methanation. *Applied Energy*, *212*, 1191–1202. https://doi.org/10.1016/j.apenergy.2017.12.099

Zhang, C., & Xu, Y. (2020). Economic analysis of large-scale farm biogas power generation system considering environmental benefits based on LCA: A case study in China. *Journal of Cleaner Production*, *258*, 120985. https://doi.org/10.1016/j.jclepro.2020.120985

Mathematical modeling of pollutant transport in river Fena in Ghana

Ferdinard Obeng-Forson[1], Joseph K. Ansong[1*]

[1]Department of Mathematics, University of Ghana, Legon, Ghana.
***Corresponding Author:** jkansong@ug.edu.gh

Abstract

In this study, we derived two analytical solutions to a one-dimensional Advection-Diffusion Equation (ADE). The ADE is solved using a constant and exponentially decaying inlet boundary condition, together with Dirichlet and Neumann outlet conditions. The analytic solutions are shown to be simple if a combination of the initial concentration and the transformed boundary condition results in a non-zero singularity pole of inverse Laplace transform. The differences between the two analytic solutions are elucidated. Moreover, the analytical solutions are compared to some observational data from the Fena River in the Ashanti region of Ghana where illegal mining activities (locally referred to as "galamsey") have been reported. The analytical results well capture the concentration of iron at two sampling locations for both the Dirichlet and Neumann models but poorly predict the concentration at a third location. Some possible reasons for this discrepancy have been hypothesized for future investigations.

Introduction

Water is essential to our existence and survival and its importance cannot be overstated. Rivers, being the most significant sources of water, are the lifeblood of humans. Not only does a river act as a primary source of irrigation for the majority of agricultural communities across the globe, but it also supplies clean and fresh water for daily necessities of living.

One major issue that poses a serious threat to both human life and the aquatic ecosystem is water pollution. Water pollution occurs when hazardous substances, such as chemicals or microbes, infiltrate an ocean, lake, stream, aquifer, or a river body, deteriorating water quality and making it harmful to humans or the environment. According to the Ghana Water Resource Commission, nearly 60% of water bodies in Ghana are polluted due to illegal mining and inappropriate agriculture methods (Mubarik, 2017). The discharge of waste substances, which contain hazardous compounds such as mercury and other organic chemicals used in mineral ores processing in mining activities. These waste substances contribute heavily to water pollution in Ghana, posing a greater threat to aquatic life and the human population that relies on such resources (Duncan et al., 2020). According to the Ministry of Lands and Natural resources, Ghana risks importing water as illegal miners devastate the country's rivers (Ghanaian Times, 2022). Once river bodies become polluted it is extremely difficult to clean up.

The transport of pollutants in rivers has become a matter of concern for environmental engineers and scientists as well as mathematical modelers. The effective control of these pollutants is critical for efficient management of their impact on the environment (Zoppou & Knight, 1997). The concentration of these pollutants released into water bodies may be described by an Advection-Diffusion Equation (ADE), a partial differential equation of parabolic type. The ADE describes a physical phenomenon whereby contaminants or other unwanted substances are transported inside a physical system due to two processes: advection and diffusion. The ADE has extensively been used to model water pollution phenomenon (Schaffner et al., 2009, Genuchten et al., 2013, Manitcharoen & Pimpunchat, 2020). It also has

a wide range of applications in many engineering fields such as modeling atmospheric pollutants (Costa et al., 2006, Moreira et al., 2006), tracer dispersion in a porous medium (Ogata & Banks 1961), and the intrusion of salt water into freshwater aquifers (Essink, 2001).

Obtaining analytic solutions to the Advection-Diffusion Equation is of great importance in mathematics. Analytical solutions are especially critical for validating solutions of the ADE obtained using numerical methods. Many analytical solutions along with varying initial and boundary conditions have been developed to quantitatively describe the one-dimensional ADE with constant coefficients. A one-dimensional (1D) single-ion ADE, which involves terms accounting for zero-order production, linear equilibrium adsorption, and first-order decay, was solved analytically by Van Genuchten (1982). Mohsen and Baluch (1983) provided an analytic solution to a 1D ADE for fixed concentration boundary conditions over a finite domain. The transformed equation was decomposed into two components and separation of variables was used to obtain the required result. Davis (1985), using a Laplace transform technique, provided two distinct analytic solutions to a single ADE over a finite domain. One solution was found to be continuous at both ends of the domain, and the other is discontinuous at the origin. In other to resolve the discontinuity at the origin, he compared the discontinuous analytic solution to the one provided by Mohsen and Baluch (1983) in Eq (20) of his paper. He found that his results and that of Mohsen and Baluch (1983) were the same but was incorrectly given as the negative of his solution. He stated that the discontinuity at the origin in the equation was due to the Fourier sine series expansion for the ratio of hyperbolic sines. In a semi-infinite domain where the diffusion coefficient is proportional to the square of the spatially dependent velocity, Kumar et al., (2012) presented an analytic solution to a 1D ADE with variable coefficients using the Laplace transform technique. Mojtabi and Deville (2015) also provided an analytical solution to a one-dimensional ADE using separation of variables but with a sinusoidal initial condition and a homogeneous boundary condition. Using a one-sided Laplace transform, Kim (2020) provided analytic solutions to a 1D Convection-Diffusion Reaction Source (CDRS) equation without explicitly computing the inverse Laplace transform. The CDRS equation was solved for both Dirichlet/Dirichlet and Dirichlet/Neumann boundary conditions together with a constant initial condition. Unlike most previous research on the ADE, few have provided analytical solutions to a one-dimensional ADE subject to an exponentially decaying boundary condition.

This paper presents analytic solutions to a one-dimensional ADE using constant initial condition and an exponentially decaying inlet boundary condition, together with Dirichlet and Neumann outlet conditions. Without directly computing the inverse Laplace transform, solutions to the ADE are obtained using the Laplace transform technique and the residue theorem approach in complex analysis as employed in Kim (2020). Additionally, the analytical solutions are compared to some observational data and the differences between the two are discussed.

Background Theory

The one-dimensional Advection-Diffusion Equation, with constant coefficients which is derived from the principle of mass conservation, is given by

$$\frac{\partial C}{\partial t} + V_0 \frac{\partial C}{\partial x} = D_0 \frac{\partial^2 C}{\partial x^2}, \tag{1}$$

where C is the concentration at a position, x and time t, and V_0 and D_0 are the constant advective velocity and diffusion, respectively. Using the dimensionless quantities defined by

$$\phi(\xi,\tau) = C(x,t)/C_0, \quad \tau = tD_0/L^2,$$

$$\xi = x/L, \quad P_e = 2\lambda = LV_0/D_0,$$

where C_0 is a reference concentration, L is a length scale of the space coordinate and $P_e = 2\lambda$ is the Peclet number, the dimensionless form of the ADE in Eq. (1) becomes

$$\frac{\partial \phi}{\partial \tau} = \frac{\partial^2 \phi}{\partial \xi^2} - 2\lambda \frac{\partial \phi}{\partial \xi} . \quad (2)$$

We next introduce and discuss two analytical solutions to the 1D ADE with Dirichlet boundary condition (referred to as Dirichlet Model) and Neumann boundary condition (referred to as Neumann Model).

Dirichlet Model

The equation to be solved is

$$\frac{\partial \phi}{\partial \tau} = \frac{\partial^2 \phi}{\partial \xi^2} - 2\lambda \frac{\partial \phi}{\partial \xi} , \quad 0 \le \xi \le 1, \quad (3)$$

subject to boundary conditions (BCs):

$$\begin{aligned} \phi(0,\tau) &= \phi_0 e^{-\gamma\tau} , \\ \phi(1,\tau) &= \phi_1 , \end{aligned} \quad (4)$$

and initial condition

$$\phi(\xi,0) = \omega_0 . \quad (5)$$

The choice of the exponentially decaying inlet BC is motivated by observational data in Fena River in Ghana (Duncan et al., 2020), where the pollutant at the inlet appears to be decaying in time as shown later.

Applying the Laplace transform

$$\Phi(\xi,p) := \mathcal{L}[\phi(\xi,\cdot)](p) = \int_0^\infty e^{-p\tau}\,\phi(\xi,\tau)\,d\tau \quad (6)$$

to Eq. (3) gives a second order ordinary differential equation

$$\frac{d^2\Phi}{d\xi^2} - 2\lambda \frac{d\Phi}{d\xi} - p\Phi = -\omega_0 \quad (7)$$

$$\left[\mathfrak{D}_\xi - \lambda_m\right]\left[\mathfrak{D}_\xi - \lambda_p\right]\Phi = -\omega_0 , \quad (8)$$

where

$$\mathfrak{D}_\xi = \frac{d}{d\xi} , \ \lambda_m = \lambda - \beta , \lambda_p = \lambda + \beta \text{ and } \beta = \sqrt{\lambda^2 + p} .$$

Define a new function as:

$$\Phi^\dagger := \left[\mathfrak{D}_\xi - \lambda_p\right]\Phi = e^{\lambda_p \xi}\mathfrak{D}_\xi\left(\Phi e^{-\lambda_p \xi}\right). \quad (9)$$

We now write Eq. (8) as

$$e^{\lambda_m \xi}\mathfrak{D}_\xi\left(\Phi^\dagger e^{-\lambda_m \xi}\right) = -\omega_0 . \quad (10)$$

The general solution for $\Phi^\dagger$ is

$$\Phi^\dagger = B_1 e^{\lambda_m \xi} + \frac{\omega_0}{\lambda_m} . \quad (11)$$

Substituting Eq. (11) into Eq. (9) gives the general solution for $\Phi(\xi,p)$ as

$$\Phi(\xi,p) = B_1 e^{\lambda_m \xi} + B_2 e^{\lambda_p \xi} + \frac{\omega_0}{p} \quad (12)$$

where

$$\Phi(0,p) = \frac{\phi_0}{p+\gamma} \text{ and } \Phi(1,p) = \frac{\phi_1}{p} . \quad (13)$$

Applying Eq. (13) above to Eq. (12) gives

$$B_1 = \frac{\left(\frac{\phi_0}{p+\gamma} - \frac{\omega_0}{p}\right)e^{\beta} - \left(\frac{\phi_1}{p} - \frac{\omega_0}{p}\right)e^{-\lambda}}{2\sinh\beta} , \quad (14)$$

$$B_2 = \frac{\left(\frac{\phi_1}{p} - \frac{\omega_0}{p}\right)e^{-\lambda} - \left(\frac{\phi_0}{p+\gamma} - \frac{\omega_0}{p}\right)e^{-\beta}}{2\sinh\beta} . \quad (15)$$

Substituting the values of B_1 and B_2 into Eq. (12) gives the general solution in terms of p as

$$\Phi(\xi,p) = \left[\frac{\phi_0 \sinh[\beta(1-\xi)]}{\sinh\beta}\right]\frac{e^{\lambda\xi}}{p+\gamma} + \left[\frac{\phi_1 e^{-\lambda}\sinh(\beta\xi)}{\sinh\beta}\right]\frac{e^{\lambda\xi}}{p}$$

$$- \left[\frac{\omega_0 \sinh[\beta(1-\xi)] + \omega_0 e^{-\lambda}\sinh(\beta\xi)}{\sinh\beta}\right]\frac{e^{\lambda\xi}}{p} + \frac{\omega_0}{p}. \quad (16)$$

To solve Eq. (16), one must apply the inverse Laplace transform (iLT) defined below which involves the method of contour integration and calculus of residues.

$$\phi(\xi,\tau) = \mathcal{L}^{-1}[\Phi(\xi,\cdot)](\tau) = \frac{1}{2\pi i}\int_{c-i\infty}^{c+i\infty} e^{\tau z}\Phi(\xi,z)dz.$$

However, this approach is most often difficult to use. Here, we apply the method devised by Kim (2020) which states that if a Laplace transformed function has only two singularity poles, $z = z_0$ (contributing to the steady-state solution) and $z = z_1$ (contributing to the transient behaviour), then the inverse Laplace transform can be avoided by applying the initial condition. To apply this method, we first let

$$\Phi_{BC}(\xi,p) = \left[\frac{\phi_0 \sinh[\beta(1-\xi)]}{\sinh\beta}\right]\frac{e^{\lambda\xi}}{p+\gamma} + \left[\frac{\phi_1 e^{-\lambda}\sinh(\beta\xi)}{\sinh\beta}\right]\frac{e^{\lambda\xi}}{p}$$

$$\Phi_{IC}(\xi,p) = -\left[\frac{\omega_0 \sinh[\beta(1-\xi)] + \omega_0 e^{-\lambda}\sinh(\beta\xi)}{\sinh\beta}\right]\frac{e^{\lambda\xi}}{p} + \frac{\omega_0}{p},$$

and also let

$$\Phi_{BC_1}(\xi,p) = \left[\frac{\phi_0 \sinh[\beta(1-\xi)]}{\sinh\beta}\right]\frac{e^{\lambda\xi}}{p+\gamma},$$

$$\Phi_{BC_2}(\xi,p) = \left[\frac{\phi_1 e^{-\lambda}\sinh(\beta\xi)}{\sinh\beta}\right]\frac{e^{\lambda\xi}}{p},$$

where Φ_{BC_1}, Φ_{BC_2} and Φ_{IC} are partial solutions of Φ.. We replace the Laplace parameter p by the complex variable z and write the iLT of Eq. (16) as

$$\phi(\xi,\tau) = \mathcal{L}^{-1}[\Phi(\xi,\cdot)](\tau) = \frac{1}{2\pi i}\int_{c-i\infty}^{c+i\infty} e^{\tau z}\Phi(\xi,z)dz$$

$$= \mathrm{Res}\left[\exp(\tau z)\Phi_{BC_1}(\xi,z) + \exp(\tau z)\Phi_{BC_2}(\xi,z) + \exp(\tau z)\Phi_{IC}(\xi,z)\right].$$

The expressions $\exp(\tau z)\Phi_{BC_1}(\xi, z)$, $\exp(\tau z)\Phi_{BC_2}(\xi, z)$ and $\exp(\tau z)\Phi_{IC}(\xi, z)$ have simple poles at $z = 0$ and $z = -\gamma$.

The Residue of $\exp(\tau z)\Phi_{BC}(\xi, z)$ and $\exp(\tau z)\Phi_{IC}(\xi, z)$ at the simple poles are calculated as follows:

$$\text{Res}(\Phi, \text{z} = -\gamma) = \lim_{z \to -\gamma}\left[(z+\gamma)\Phi_{BC_1}(\xi, z)e^{\tau z}\right] = f_{B_1}e^{\lambda\xi - \gamma\tau},$$

where

$$f_{B_1} = \left[\frac{\phi_0 \sinh \omega(1-\xi)}{\sinh \omega}\right] \tag{17}$$

and $\omega = \sqrt{\lambda^2 - \gamma}$. For physically relevant solutions, we suppose that $\lambda^2 > \gamma$. Solutions for the case where $\lambda^2 < \gamma$ can be derived (see Obeng-Forson, 2022) but yield unrealistic values.

Similarly,

$$\text{Res}(\Phi, \text{z} = 0) = \lim_{z \to 0}\left[z\Phi_{BC_2}(\xi, z)e^{\tau z}\right] = f_{B_2}e^{\lambda\xi},$$

where

$$f_{B_2} = \left[\frac{\phi_1 e^{-\lambda} \sinh(\lambda\,\xi)}{\sinh \lambda}\right]. \tag{18}$$

Also,

$$\text{Res}(\Phi, \text{z} = 0) = \lim_{z \to 0}[z\Phi_{IC}(\xi, z)e^{\tau z}] = -f_C e^{\lambda\xi} + \omega_0\ ,$$

where

$$f_C = \frac{\omega_0 \sinh[\lambda(1-\xi)] + \omega_0 e^{-\lambda}\sinh(\lambda\xi)}{\sinh \lambda}\ . \tag{19}$$

Besides, $\Phi_{BC}(\xi, z)$ and $\Phi_{IC}(\xi, z)$ have the same pole when

$$\sinh \beta = 0 \implies z = -\lambda^2.$$

The Residues at $z = -\lambda^2$ are calculated below. That of $\exp(\tau z)\Phi_{BC_1}(\xi, z)$ is calculated as

$$\lim_{z \to -\lambda^2}\left[(z+\lambda^2)e^{\tau z}\Phi_{BC_1}(\xi, z)\right] = -\frac{e^{\lambda\xi - \lambda^2\tau}}{\lambda^2 - \gamma}\,\mathcal{R}\left[f_{B_1}\right],$$

where

$$\mathcal{R}\left[f_{B_1}\right] = \lim_{z\to-\lambda^2}(z+\lambda^2)\left(\frac{\phi_0 \sinh \beta(1-\xi)}{\sinh\beta}\right)$$

and $\beta = \sqrt{\lambda^2 + z}$.

Similarly, the Residue of $\exp(\tau z)\Phi_{BC_2}(\xi, z)$ is calculated as

$$\lim_{z\to-\lambda^2}\left[(z+\lambda^2)e^{\tau z}\Phi_{BC_2}(\xi,z)\right] = -\frac{e^{\lambda\xi-\lambda^2\tau}}{\lambda^2}\,\mathcal{R}\left[f_{B_2}\right]$$

where

$$\mathcal{R}\left[f_{B_2}\right] = \lim_{z\to-\lambda^2}(z+\lambda^2)\left(\frac{\phi_1 e^{-\lambda} \sinh(\beta\,\xi)}{\sinh\beta}\right).$$

Lastly, the residue of $\exp(\tau z)\Phi_{IC}(\xi, z)$ is

$$\lim_{z\to-\lambda^2}[(z+\lambda^2)e^{\tau z}\Phi_{IC}(\xi,z)] = \frac{e^{\lambda\xi-\lambda^2\tau}}{\lambda^2}\,\mathcal{R}[f_C]$$

where

$$\mathcal{R}[f_C] = \lim_{z\to-\lambda^2}(z+\lambda^2)\left(\frac{\omega_0 \sinh[\beta(1-\xi)] + \omega_0 e^{-\lambda}\sinh(\beta\xi)}{\sinh\beta}\right)$$

and $\mathcal{R}[f]$ indicates the specific residue to be calculated for $z = -\lambda^2$.

Using the calculated residues, the solution can now be written in terms of τ as

$$\begin{aligned}\phi(\xi,\tau) = f_{B_1}e^{\lambda\xi-\gamma\tau} + f_{B_2}e^{\lambda\xi} - f_C e^{\lambda\xi} - (\lambda^2-\gamma)^{-1}e^{\lambda\xi-\lambda^2\tau}\,\mathcal{R}\left[f_{B_1}\right] \\ -\lambda^{-2}e^{\lambda\xi-\lambda^2\tau}\,\mathcal{R}\left[f_{B_2}\right] + \lambda^{-2}e^{\lambda\xi-\lambda^2\tau}\,\mathcal{R}[f_C] + \omega_0 \qquad (20)\end{aligned}$$

where the residues $\mathcal{R}[f]$ are still unknown.

A major step in the solution approach is to apply the initial condition $\phi(\xi, 0) = \omega_0$ to Eq.(20) to calculate for the residues.

This gives

$$(\lambda^2-\gamma)^{-1}\,\mathcal{R}\left[f_{B_1}\right] + \lambda^{-2}\mathcal{R}\left[f_{B_2}\right] - \lambda^{-2}\mathcal{R}[f_C] = f_{B_1} + f_{B_2} - f_C\,, \qquad (21)$$

and substituting Eq. (21) into Eq. (20) gives

$$\begin{aligned}\phi(\xi,\tau) &= f_{B_1}e^{\lambda\xi-\gamma\tau} + f_{B_2}e^{\lambda\xi} - f_C e^{\lambda\xi} - \left(f_{B_1} + f_{B_2} - f_C\right)e^{\lambda\xi-\lambda^2\tau} + \omega_0 \\ &= f_{B_1}\left[e^{-\gamma\tau} - e^{-\lambda^2\tau}\right]e^{\lambda\xi} + f_{B_2}\left[1 - e^{-\lambda^2\tau}\right]e^{\lambda\xi} - f_C\left[1 - e^{-\lambda^2\tau}\right]e^{\lambda\xi} + \omega_0\end{aligned} \tag{22}$$

Substituting Eq. (17), Eq. (18) and Eq. (19) into Eq. (22) yields

$$\begin{aligned}\phi(\xi,\tau) = \frac{\phi_0 \sinh\omega(1-\xi)}{\sinh\omega}\left[e^{-\gamma\tau} - e^{-\lambda^2\tau}\right]e^{\lambda\xi} + \frac{\phi_1 e^{-\lambda}\sinh(\lambda\xi)}{\sinh\lambda}\left[1 - e^{-\lambda^2\tau}\right]e^{\lambda\xi} \\ -\omega_0\left(\frac{\sinh\lambda(1-\xi) + e^{-\lambda}\sinh(\lambda\xi)}{\sinh\lambda}\right)\left[1 - e^{-\lambda^2\tau}\right]e^{\lambda\xi} + \omega_0.\end{aligned} \tag{23}$$

The steady-state solution for $\phi(\xi,\tau)$ is given as

$$\phi_{ss}(\xi) = \frac{\phi_1 e^{-\lambda}\sinh(\lambda\xi)}{\sinh\lambda}e^{\lambda\xi} - \omega_0\left(\frac{\sinh\lambda(1-\xi) + e^{-\lambda}\sinh(\lambda\xi)}{\sinh\lambda}\right)e^{\lambda\xi} + \omega_0$$

The solution for $\phi(\xi,\tau)$ holds for $0 < \xi < 1$ but it does not satisfy the conditions at the boundaries in general. However, it can be shown that to satisfy the inlet boundary condition, we must have $\omega_0 = \phi_0$. Similarly, to satisfy only the outlet condition one must have $\omega_0 = \phi_1$.

When $\gamma = 0$ we recover the general solution provided by Kim (2020) (Eq. (8) in his paper for $\kappa = 0$ and $\sigma = 0$.)

Figure 1 shows plots of Eq. (23) for fixed values of τ. When $\gamma = 0$, we recover the solution of Kim (2020) as displayed in Figure 1A. In this case, the concentration everywhere within the domain increases with time until the system reaches steady state, with concentration decreasing monotonically from the inlet to the outlet.

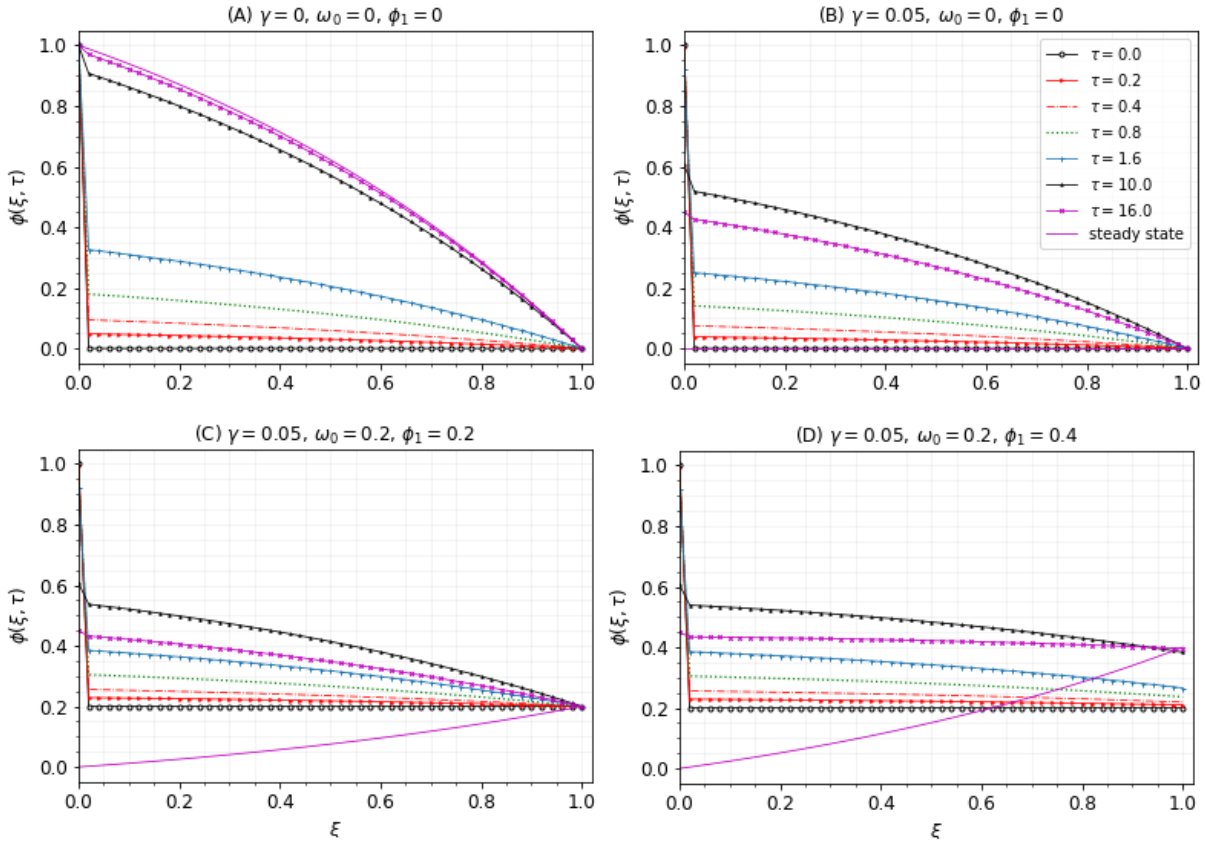

Figure 1: *Concentration at different times for* $\lambda = 0.5$, $\phi_0 = 1$ and (A) $\gamma = 0$, $\omega_0 = 0 = \phi_1$ (B) $\gamma = 0.05, \omega_0 = 0 = \phi_1$ (C) $\gamma = 0.05, \omega_0 = 0, \phi_1 = 0.2$ and (D) $\gamma = 0.05, \omega_0 = 0.2$, $\phi_1 = 0.4$.

However, in the presence of a decaying inlet condition with a Dirichlet outlet condition, the time evolution of concentration behaves differently from the case for which $\gamma = 0$ as seen in Figure 1B. Initially the concentration is zero except at the inlet where it has a maximum value of $\phi(\xi, 0) = \phi_0 = 1$. As time evolves, the concentration at the inlet begins to decrease while the concentration everywhere within the domain increases, with a monotonically decreasing shape as in Figure 1A. The concentration within the domain increases to a maximum point (around $\tau = 10$ in this case) and begins to decrease (see the curve for $\tau = 16$) and eventually goes to zero everywhere at steady-state.

If both the initial concentration and γ are non-zero (e.g., $\omega_0 = \phi_1 = 0.2$, $\gamma = 0.05$), the solution behaves similarly to the case for $\omega_0 = 0$ (Figure 1B), but the rate of increase of ϕ within the domain to the maximum point is much faster (Figure 1C), since the initial concentration is non-zero. Moreover, the steady state solution is not zero everywhere as in the previous case but increases gradually from zero at the inlet to the value at the outlet. Thus, in

this case, the concentration can decrease below the initial concentration due to the exponentially decreasing condition at the inlet. A more general case in which the initial condition and outlet value are non-zero and different from each other is shown in Figure 1D. The concentration increases to a maximum value as in Figures 1B-C, but tends to converge at the outlet value ($\phi_1 = 0.4$ in this case).

Neumann Model

The equation to be solved is

$$\frac{\partial \phi}{\partial \tau} = \frac{\partial^2 \phi}{\partial \xi^2} - 2\lambda \frac{\partial \phi}{\partial \xi}, \quad 0 \le \xi \le 1,$$

subject to BCs

$$\begin{aligned} \phi(0,\tau) &= \phi_0 e^{-\gamma\tau} \ , \\ \frac{\partial \phi(1,\tau)}{\partial \xi} &= J_1 \ , \end{aligned} \tag{24}$$

and initial condition

$$\phi(\xi, 0) = \omega_0 \ . \tag{25}$$

Using the same procedure as in the Dirichlet model, the analytical solution to the Neumann model is (Obeng-Forson, 2022)

$$\begin{aligned} \phi(\xi,\tau) = {} & \frac{J_1 e^{-\lambda} \sinh \lambda\xi}{\lambda \sinh\lambda + \lambda\cosh\lambda}\left[1 - \ e^{-\lambda^2\tau}\right] e^{\lambda\xi} \\ & + \frac{\phi_0 \lambda \sinh\omega(1-\xi) + \phi_0 \omega \cosh\omega(1-\xi)}{\lambda\sinh\omega + \omega\cosh\omega}\left[\ e^{-\gamma\tau} - \ e^{-\lambda^2\tau}\right] e^{\lambda\xi} \\ & - \frac{\omega_0 \lambda\sinh\lambda(1-\xi) + \omega_0\lambda\cosh\lambda(1-\xi)}{\lambda\sinh\lambda + \lambda\cosh\lambda}\left[1 - \ e^{-\lambda^2\tau}\right] e^{\lambda\xi} + \omega_0. \end{aligned} \tag{26}$$

The steady-state solution is given as

$$\phi_{ss}(\xi) = \left(\frac{J_1 e^{-\lambda}\sinh\lambda\xi}{\lambda\sinh\lambda + \lambda\cosh\lambda}\right) e^{\lambda\xi} - \left(\frac{\omega_0\lambda\sinh\lambda(1-\xi) + \omega_0\lambda\cosh\lambda(1-\xi)}{\lambda\sinh\lambda + \lambda\cosh\lambda}\right) e^{\lambda\xi} + \omega_0. \tag{27}$$

Example plots from the solution in equations (26) and (27) can be found in Obeng-Forson (2022).

Application to the Transport of a Pollutant

We now apply our theoretical solutions to model the transport of a pollutant (iron) in the Fena River in the Ashanti region of Ghana.

Data are obtained from the published paper by Duncan et al., (2020) who conducted research in and around the Fena River to determine the levels of heavy metal pollution due to illegal mining (locally referred to as "galamsay") activities. They took samples from five locations: Fenaso No. 1 (referred to as Fen-1), Fenaso No. 2 (referred to as Fen-2), Point A, Point B, Point C, and Fenaso No. 3 (referred to as Fen-3), in that order from north to south. Thus, the river flows southward from Fen-1 through Fen-3 until it enters the Gulf of Guinea in the Atlantic Ocean. A map of the area and sampling points can be seen in their Figure 1. The sampling points at Fen-1 and Fen-2 are very close to each other. According to Duncan et al., (2020), there were illegal mining activities in and around all the sampling locations except sampling Point A where there was no apparent mining activity going on. The three main heavy metal pollutants in the river; exceeding safe drinking water guidelines, were found to be Cadmium (Cd), Lead (Pb) and Iron (Fe) (Duncan et al., 2020). Here, we focus on modeling the transport of Iron, because the initial and boundary data roughly match our theoretical set up.

The monthly concentration of Iron at three locations (Fen-1, Fen-2 and Point-A, obtained from Table 3 of Duncan et al., 2020) over the one-year period of their study (from January to December in 2020) is shown in Figure 2. We display only three locations because we are interested in modeling concentrations at Fen-2 and Point-A. We are particularly interested in Point-A because it was reported that there was no apparent illegal mining activity at the location, so we assume that the concentration of Fe at Point-A is likely due to upstream effects. The highest concentrations occur at Fen-1 and Fen-2 with the smallest concentrations of Fe at Point-C (not shown). The concentration of Fe at Fen-1 is generally decreasing with time over the study period (Figure 2a).

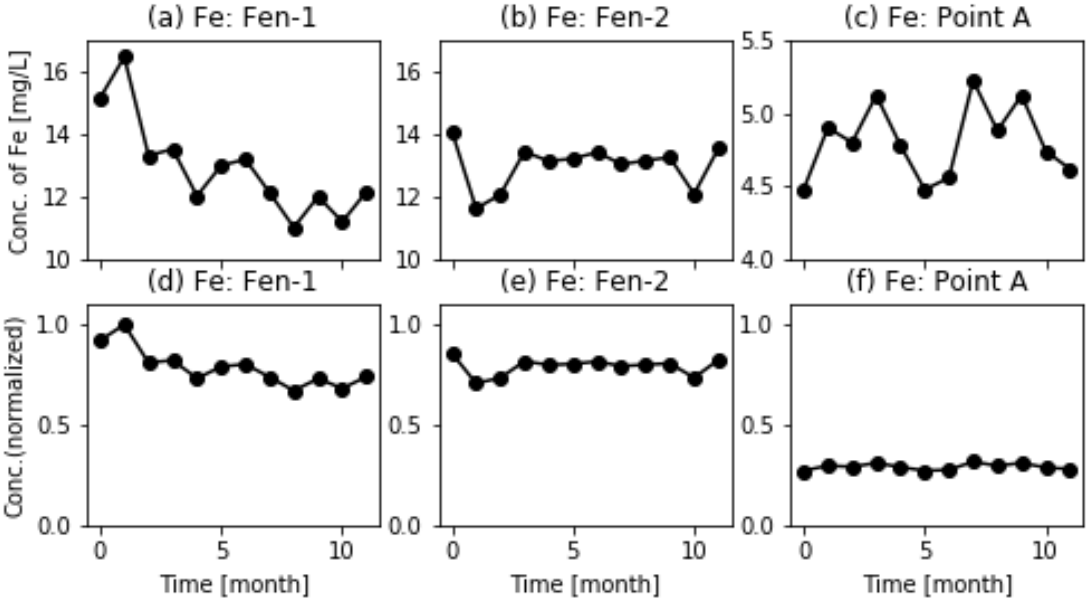

Figure 2 *[Row 1] Variation of Iron (Fe) concentration over time in Fena river (as reported in Table 3 of Duncan* et al.*, 2020). The vertical scales are different to highlight variability in concentrations. [Row 2] Same as Row 1 but for normalized concentrations*.

Methodology and diffusion coefficient estimation

To apply our mathematical models, we normalized the concentrations by the highest concentration at Fen-1 (see Figure 3). The concentration at the inlet is taken to be the concentrations at Fen-1 while the initial concentration is taken to be that of January at all locations. The measured concentration of Fe in January is depicted in Figure 3 (left panel).

The parameter λ in the governing equation is related to the Peclet number $Pe = 2\lambda$ with $\lambda = LV_0/D_0$, where L is the length scale of the domain, V_0 is the averaged velocity of the flow and D_0 is a constant diffusion coefficient. We estimated the velocity, V_0 of the river to be 2m/s, by taking videos of the flow and measuring the speed of floating objects. We also measured the average width, W of the river around the same location to be ~5.2m and the average depth, H to be 1.0 m. So, the average discharge, $Q = HWV_0$, at the location is about $10.4 m^3/s$.

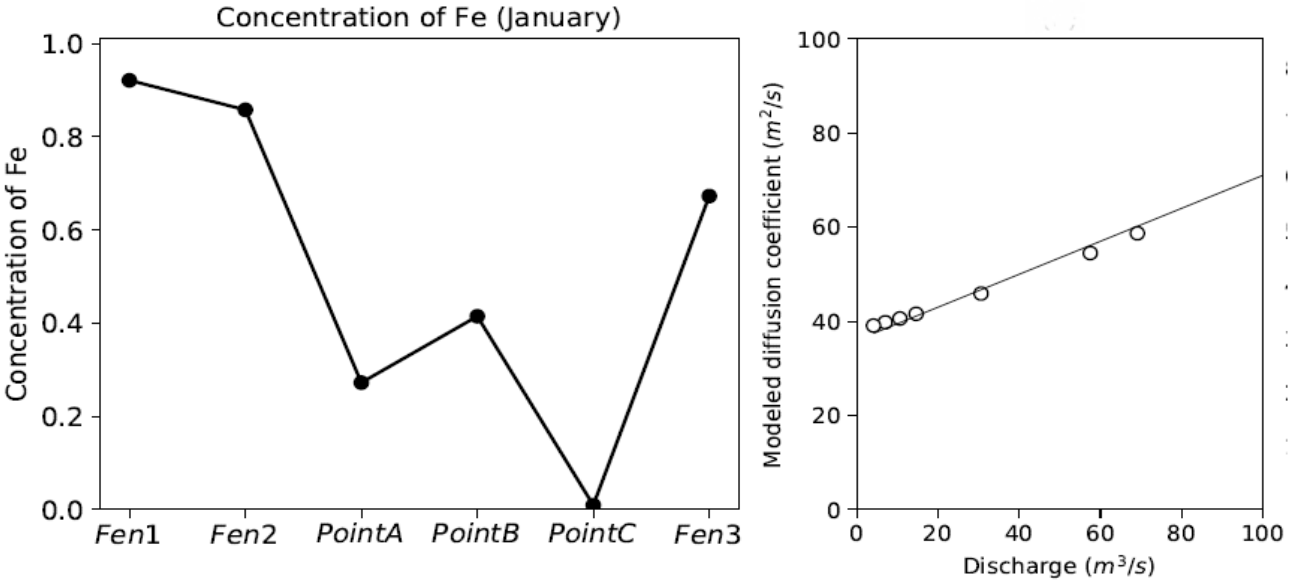

Figure 3: Normalized concentration of Fe in January at all sampling points (left panel) and the right panel shows Diffusion coefficient as a function of discharge from Table 7 (case 2) of Tayfur and Singh (2005) for D_0<100 m^2/s.

Besides the velocity, the parameter that plays a much more critical role in modeling the transport of pollutants in streams and rivers is the longitudinal diffusion coefficient, D_0. Once a pollutant is released into a river or flowing water body, it undergoes various stages of mixing with the ambient water. After the contaminant is mixed in the cross-sectional direction, the most important process is the longitudinal dispersion which is measured by the longitudinal dispersion coefficient (Tayfur & Singh, 2005). Tayfur and Singh (2005) developed a model based on Artificial Neural Network (ANN) for predicting the longitudinal dispersion coefficient. Among other things, they reported that the discharge data alone is sufficient for computing the dispersion coefficient for more frequently occurring low values of the dispersion coefficient D_0<100 m^2/s. We fitted lines to their data points that are closest to the observed data (see their Table 7, case 2) to get the diffusion coefficient, D, as a function of discharge to be

$$D = 0.35Q + 36 \text{ for } Q \leq 110, \qquad (28)$$

as depicted in Figure 3 (right panel). Using the formula in Eq. (28), we estimate the value of the longitudinal dispersion in Fena River to be 39.6 m^2/s. Thus, the Peclet number is 389 and the parameter $\lambda \approx 194.5$.

Comparison of model results to observational data

We compared the observational data of iron (Fe) concentration in Fena River with the Dirichlet model. The initial concentration $\omega_0=0.52$ is taken to be the average concentration at all locations in January (see Figure 3, left panel). In each case, the inlet boundary is an exponentially decreasing concentration of the form $\phi_0 e^{-\gamma\tau}$ where $\phi_0=1$. By fitting an exponentially decreasing function to the data at Fen-1 (see Figure 2a), we get $\gamma=0.025$.

We plot the model results against the observational data of Fe in the Fena River for Fen-1, Fen-2, and Point A after estimating all parameters in the analytical solution of the Dirichlet model, Eq. (23). Note that the e τ values are calculated from the dimensionless equation, $\tau=tD_0/L^2$, where L = 7700 m is the estimated length scale of the spatial domain.

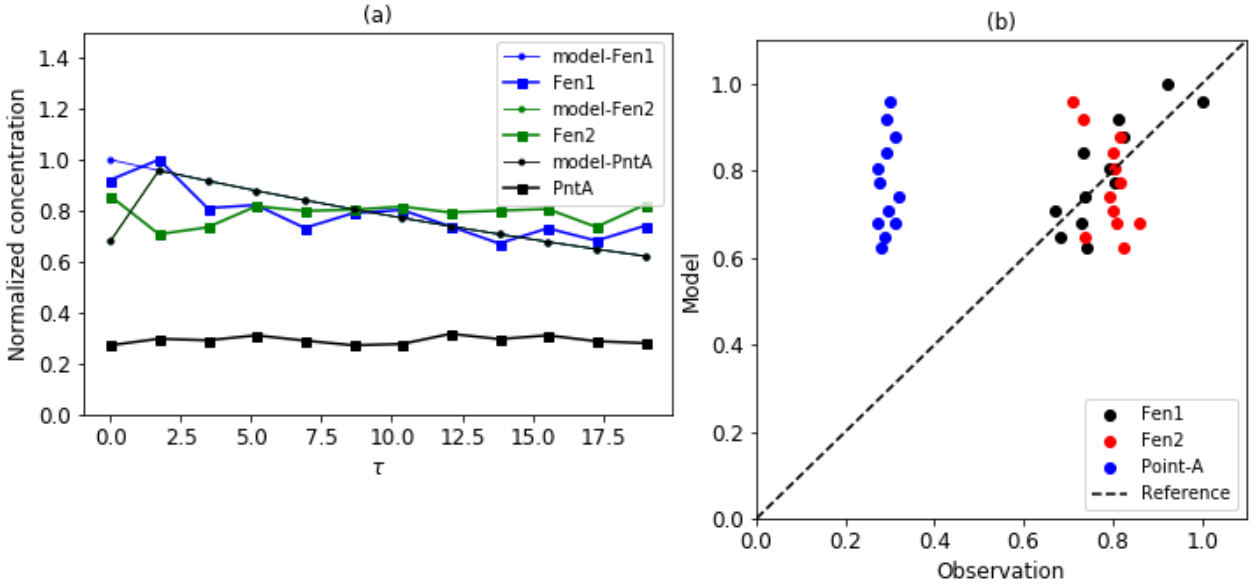

Figure 4: Temporal variation of observed and Dirichlet model concentrations at Fen-1, Fen-2 and Point-A.

The concentration of iron as a function of time from both the observational data and Dirichlet model is shown in Figure 4a. Apart from the initial time, the model results at Fen-1, Fen-2 and Point-A are indistinguishable from each other. The model captures the concentrations at Fen-1 and Fen-2 relatively well since these locations are closer to each other, and data from Fen-1 is used as the inlet boundary condition. However, the model predicts very large concentrations at Point-A. We conjecture a couple of reasons that may account for the higher modelled concentrations at Point-A. Firstly, Fen-1 and Fen-2 are not directly located on the river, so it is likely that we overestimated the concentrations there, resulting in higher concentrations at Point-A. Secondly, we notice that the normalized concentrations at Point-A are generally constant around a mean value of 0.25 (also see Figure 2f). Thus, it appears other unknown factors, besides direct transport from Fen-1 and Fen-2, maybe implicated. Thirdly, there are several uncertainties in estimating the parameters that went into applying our

model to the observational data. For instance, the speed of the flow varies both in space and time, but this is neither captured in the model nor our observed speed. Finally, another reason could be the fact that the model is one-dimensional and so does not capture lateral dispersion of pollutants which is likely to reduce the concentration of Iron at Point-A if direct transport is the principal mechanism.

The comparison of the Neumann model to the observations is not very different from that of the Dirichlet model, so we do not show that here (see Obeng-Forson, 2022).

Conclusions

We derived analytical solutions to the 1D Advection-Diffusion Equation with exponentially decaying inlet boundary condition. This was motivated by observational data in Fena River in the Ashanti Region of Ghana where illegal mining activities (locally referred to as "galamsey") have been reported. Using the Laplace transform technique, the analytical solutions were obtained without directly computing the inverse Laplace transform of the transformed equation following work by Kim (2020). Additionally, our analytical solutions were compared to the observed data of pollutants (iron in this case) from Fena River. We found that the analytical results well capture the concentration of iron at two sampling locations, Fen-1 and Fen-2, as shown in Figure 4. However, the model results predicted very large concentrations at Point-A. We have given several reasons that could be responsible for this discrepancy. These include, but not limited to, the fact that (1) the initial source concentrations used in our model might be overestimated, (2) the one-dimensional nature of the model limits lateral dispersion, and (3) other factors, other than direct transport from Fen-1 and Fen-2, might be at play at Point-A. In the future, we plan to model the advection and diffusion of some of the other chemicals found in the river.

References

Costa, C., Vilhena, M., Moreira, D., & Tirabassi, T. (2006). Semi- analytical solution of the steady three-dimensional advection-diffusion equation in the planetary boundary layer. *Atmospheric Environment*, *40*(29):5659–5669.

Davis, G. (1985). A Laplace transform technique for the analytical solution of a diffusion-convection equation over a finite domain. *Applied Mathematical Modelling*, *9*(1):69–71.

Duncan, A. E. (2020). The Dangerous Couple: Illegal Minining and Water Pollution - A Case Study in Fena River in the Ashanti Region of Ghana. *Journal of Chemistry*.

Essink, G. H. O. (2001). Improving fresh groundwater supply-problems and solutions. *Ocean & Coastal Management*, *44*(5-6):429–449.

Genuchten, M. T., Leij, F. J., Skaggs, T. H., Toride, N., Bradford, S. A., & Pontedeiro, E. M. (2013). Exact analytical solutions for contaminant transport in rivers 1. the equilibrium advection-dispersion equation. *Journal of Hydrology and Hydromechanics*, *61*(2):146.

Ghanaian Times, (May, 2022). Ghana risks importing water if… https://www.ghanaiantimes.com.gh/ghana-risk-importing-water-if.

Kim, A. S. (2020). Complete analytic solutions for convection-diffusion- reaction-source equations without using an inverse laplace transform. *Scientific Reports*, *10*(1):1–13.

Kumar, A., Jaiswal, D. K., & Yadav, R. R. (2012). Analytical solutions of one-dimensional temporally dependent advection-diffusion equation along longitudinal semi-infinite homogeneous porous domain for uniform flow. *Journal of Mathematics*, *2*, 1–11.

Manitcharoen, N. & Pimpunchat, B. (2020). Analytical and numerical solutions of pollution concentration with uniformly and exponentially increasing forms of sources. *Journal of Applied Mathematics*.

Mohsen, M. F. N. & Baluch, M. H. (1983). An analytical solution of the diffusion-convection equation over a finite domain. *Applied Mathematical Modelling, 7*(4):285–287.

Mojtabi, A. & Deville, M. O. (2015). One-dimensional linear advection–diffusion equation: Analytical and finite element solutions. *Computers & Fluids, 107,*189–195.

Moreira, D., Vilhena, M., Buske, D., & Tirabassi, T. (2006). The giltt solution of the advection–diffusion equation for an inhomogeneous and nonstationary pbl. *Atmospheric Environment, 40*(17):3186–3194.

Mubarik, A. (2017). *60% of Ghana's water bodies polluted-Water Resources Commission.* Pulse Ghana. https://www.pulse.com.gh/ece-frontpage/galamsey-60-of-ghanas-water-bodies-polluted-water-resources-commission/czgh6d8.

Obeng-Forson, F. (2022). Analytical solutions to 1D advection-diffusion equation and comparison to observations. *MPhil Thesis*, Department of Mathematics, University of Ghana, Legon.

Ogata, A. & Banks, R. B. (1961). A solution of the differential equation of longitudinal dispersion in porous media: fluid movement in earth materials. *US Government Printing Office.*

Schaffner, M., Bader, H.-P., & Scheidegger, R. (2009). Modeling the contribution of point sources and non-point sources to thachin river water pollution. *Science of the Total Environment, 407*(17):4902–4915.

Tayfur, G. & Singh, V. P. R. (2005). Predicting longitudinal dispersion coefficient in natural streams by artificial neural network. *Journal of Hydraulic Engineering*.

Van Genuchten, M. T. (1982). Analytical solutions of the one- dimensional convective-dispersive solute transport equation. Number 1661. *US Department of Agriculture, Agricultural Research Service.*

Zoppou, C. & Knight, J. (1997). Analytical solutions for advection and advection-diffusion equations with spatially variable coefficients. *Journal of Hydraulic Engineering, 123*(2):144–148.

Isotherm and Thermodynamical Studies of Arsenic Adsorption from Water using Laterite

Ebenezer Annan[1], Daniel Amusah[1], Godfred Bright Hagan[2]*, Augustine Nana Sekyi Appiah[3]

[1]Department of Materials Science and Engineering, School of Physical and Mathematical Sciences, University of Ghana, Legon, Accra, Ghana.
[2]Department of Physics, School of Physical and Mathematical Sciences, University of Ghana, Legon, Accra, Ghana.
[3]Laboratory of Materials Research, Faculty of Mechanical Engineering, Silesian University of Technology, Gliwice, Poland.

***Corresponding author:** gbhagan@ug.edu.gh

Abstract

This study investigates the removal of arsenic (As) from polluted water using laterite. Three different particle sizes 425, 850, and 106 µm of laterite were prepared, characterised and utilised as an adsorbent to remove As from polluted water. The highest removal efficiency was 94.90% and was associated with the particle size of 106 µm. The adsorption data can best be described by Langmuir Isotherm model, which had a superior *R*-square value of 0.99 to that of Freundlich adsorption model from the Isotherm modelling fitting. The results indicated that metal ion absorption occurs on a homogenous surface via monolayer adsorption and that the adsorption process may be controlled by chemisorption processes. The removal efficiency values were found to be increasing with increasing temperature. The enthalpy (ΔH°) and entropy (ΔS°) for the thermodynamical process at 308.15 K were 32.2 kJ/mol and 206.0 J/K mol, respectively, for the optimum particle size (106 µm) of the laterite. Gibb's Free Energy (ΔG°) was determined to be -31.70, -33.54, and -35.85 kJ/mol at temperatures 308.15, 318.15, and 328.15 K respectively. The negative ΔG° values reflect the feasibility and spontaneity of the adsorption process. The adsorption process can, thus, be described as endothermic. Lateritic soil adopted has a promising ability in arsenic adsorption.

Keywords: Laterite, arsenic removal, adsorption technology, thermodynamical modelling, temperature effect

Introduction

Anthropogenic sources such as mining wastes, petroleum refining, sewage sludge, agricultural chemicals, and ceramic industries play a major role in the pollution of our water bodies (Viraraghavan et al., 1999). Also, natural processes can serve as pollution sources. These include weathering, erosion of rocks, and volcanic emissions which produce pollutants into the environment. Some of these pollutants released into the water bodies largely contain heavy metals such as lead, cadmium, nickel, mercury as well as arsenic (Nagajyoti et al., 2010).

Arsenic is a naturally occurring substance present in rocks, water, air, animals, and plants. It is a kind of metalloid that can exist in both inorganic and organic forms (Matschullat, 2000). In the presence of other elements such as iron and sulphur, arsenic species may be converted into various forms or turned into insoluble compounds (Mandal & Suzuki, 2002). Arsenic compounds are mostly odourless and colourless which create an elevated health risk. A previous publication reported that arsenic is a unique carcinogen. It is the only known human carcinogen for which there is adequate evidence of carcinogenic risk by both inhalation and ingestion (Kapaj et al., 2006). Research on the source, behaviour, and distribution of arsenic in the atmosphere, as well

as its removal technique, has been conducted around the world due to its high toxicity and widespread presence in the environment. High amounts of arsenic in water have been found in many countries, including parts of the United States, China, Chile, Bangladesh, Taiwan, Mexico, Argentina, Poland, Canada, Hungary, Ghana, and Japan (Chakraborti et al., 2002; Chen et al., 1994; He & Charlet, 2013; Karim, 2000; Ning, 2002; Smedley & Kinniburgh, 2002; Wang & Mulligan, 2006). Drinking water is considered as the major intake of arsenic compounds which increases the health risk of human life. Due to its health risks and difficulty in removal, the current recommended limit for arsenic in drinking water by the World Health Organization (WHO) is 0.01 mg/L.

Processes such as oxidation (Pierce & Moore, 1982; Sorlini & Gialdini, 2010), Co-precipitation (Choong et al., 2007; Kumar et al., 2004), ion exchange (Anirudhan & Unnithan, 2007), membrane technologies (Brandhuber & Amy, 2001), and adsorption are reported to remove arsenic from water. Many of these procedures are either expensive or not effective and sometimes difficult to carry out, but adsorption has been the most promising method to remove a more reasonable quantity of arsenic compounds from water compared to the other processes (Anirudhan & Unnithan, 2007; Choong et al., 2007; Kumar et al., 2004; Sorlini & Gialdini, 2010).

Many natural and synthetic sorptive media have been identified to dissolve arsenic, including activated alumina, activated carbon, iron, and manganese coated powder, kaolinite clay, hydrated ferric oxide, activated bauxite, titanium oxide, and selenium oxide (Brandhuber & Amy, 2001). In this research, lateritic soil is used due to their high iron oxide content.

It is estimated that over 140 million people have been exposed to drinking water containing more than 10 g/L of arsenic in recent decades (Bagchi, 2007). It has been established by WHO that long-term exposure to the metalloid element arsenic can cause cancer, cardiovascular diseases, skin lesions as well as diabetes, and in the long run death. Arsenic is mainly found in water and food (Smith & Smith, 2004). While the effects of this poisonous agent are not readily visible, procedures to eliminate arsenic and have filtered water for use are being investigated. Cost-effective filtration systems have been developed to combat this arsenic contamination of water. However, these systems need expertise and prohibit easy use in developing countries due to socio-economic conditions that exist in such countries.

To address this challenge, adsorption technology, which uses raw materials and industrial waste in their natural or modified forms to remove arsenic from aqueous solutions is being explored. It is highly versatile and provides a cost-effective alternative to conventional chemical, physical remediation, and decontamination strategies (Mostafa et al., 2012). The nano-size, catalytic potential, large surface area, and high reactivity of adsorbents synthesised from local materials facilitate better arsenic removal efficiency. This research considers the use of the raw material, laterite as an adsorbent for arsenic removal. The study assesses the removal efficiency values of laterite as adsorbent and the effect of temperature on the removal efficiency of laterite along thermodynamical modelling.

Materials and Methods

Water samples was obtained from River Ankobra in the Wassa Amenfi East Municipal in the Western Region of Ghana. Figure 1 shows the geographical location of the river basin (Aduah et al., 2018).

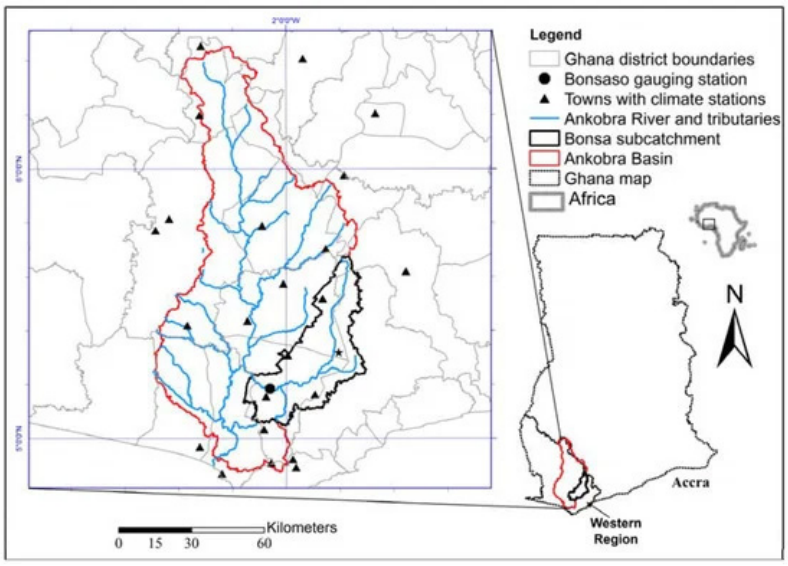

Fig. 1. Location of River Ankobra

The water samples were filtered using filter paper, frozen, and transported to the laboratory. Conc. nitric acid (16 N) was added to preserve the samples. The initial arsenic concentration in the samples was measured at the laboratory at the Ghana Standard Authority and compared to the levels after the absorption procedure.

Laterite Preparation and Characterisation

Samples of laterite soil were obtained from a road construction site at Amanfro on the Adentan-Dodowa road in the Greater Accra Region, Ghana. The laterite samples were stored in an oven at 100 °C for two hours. The samples were powdered using a mortar and pestle, and sieved into three particle sizes: 850 microns, 425 microns, and 106 microns (Figure 2)

(a) **(b)** **(c)**

Fig. 2. Preparation of laterite adsorbent: (a) Coarse laterite sampled from site (b) Sieving powdered laterite into different particle sizes (c) Weighing powdered laterite sample for batch adsorption studies

The characterisation of the laterite sample was carried out using X-ray powder diffraction (XRD), X-ray fluorescence (XRF), and Fourier Transform Infrared (FTIR). The FTIR analysis was performed using the Bruker Spectrum Two N™ (PerkinElmer, Frontier, Perkin Elmer, Ohio, USA) at laboratory of the Department of Chemistry, University of Ghana. 5 - 10 mg of the optimum particle size (106 μm) of the laterite was well compressed onto the diamond surface UATR holder of the FTIR device. The sample was scanned and ATR correction undertaken to normalise the spectrum output.

Batch Adsorption Experiment

Batch adsorption tests were performed on the polluted water sample to establish the adsorption removal efficiency ability for arsenic. A 100 mL of the polluted water sample was thoroughly mixed with a specified dosage of the adsorbent in a 250 mL flask. To ensure thorough mixing, the mixture was positioned in an orbital shaker (at a constant rate of 200 rpm) for the required contact time. The pH of the sample was measured. The mixture was then filtered, and 20 mL of the filtrate was used in determining the concentration of arsenic in the solution. Different adsorption processes were carried out to ascertain the effect of adsorption dosage, contact time, and temperature. The volume of the solution (V) was maintained throughout the experiment.

To explore the effect of adsorbent dosage on removal efficiency, various lateritic dosage (1.0 - 3.5 mg in the intervals of 0.5 mg) for the particle sizes 106, 450, and 850 μm were used. A 100 mL arsenic solution was added to each mass of adsorbent, and the mixture was agitated on a mechanical shaker spinning at 200 rpm for a maximum contact duration of 60 min.

The effect of time on removal was also investigated for the various particle sizes at optimum dosage (from 30 to 270 min at 30 min intervals). The concentration of arsenic was determined. The effect of temperature on removal of arsenic from polluted water was carried out at 35, 45, and 55 °C for the particle size that showed best removal efficiency.

Isotherm Modelling of Adsorption Data

Freundlich and Langmuir models are the basic models adopted in this research for isothermal process modelling. The Langmuir equation assumes that the maximum adsorption takes place when the surface is covered by adsorbate in a monolayer and that the point of valance exists on the surface of the adsorbent and that each of these sites (with equal affinity and independent) are capable of adsorbing one molecule. The Freundlich model is empirical.

The original and linear forms of the Langmuir and Freundlich models are given by equations (1) and (2), respectively.

Original Form	Linear Form	
$q_e = \frac{q_m \times K_L \times C_e}{1 + K_L \times C_e}$	$\frac{C_e}{q_e} = \frac{1}{K_L q_m} + \frac{1}{q_m} C_e$	(1)
$q_e = K_F \times C_e^{\,1/n}$	$\log q_e = \log K_F + \frac{1}{n} \log C_e$	(2)

where K_L and q_m are the Langmuir constant and maximum adsorption capacity (mg/g) respectively; q_e is the adsorption capacity (mg/g) at equilibrium; K_F and $(1/n)$ are the Freundlich constants; and C_e is the equilibrium concentration (mg/L).

Thermodynamical Modelling

Thermodynamic parameters, including Gibbs free energy change ($\Delta G°$), enthalpy change ($\Delta H°$) and entropy change ($\Delta S°$) serve to evaluate the effect of temperature on the adsorption of arsenic onto adsorbents and provide in-depth information regarding the inherent energy changes associated with the adsorption process (Chen & Zhang, 2014). These parameters are calculated from equations (3) – (5):

$$\Delta G° = -RT \ln K_L{}^o \quad (3)$$

where R is the universal gas constant (8.314 J/mol K), T the temperature (K), and $K_L{}^o$ the (dimensionless) 'thermodynamic' Langmuir constant for the adsorption process.

$$\ln K_L{}^o = (\Delta S°/_R) - (\Delta H°/_{RT}) \quad (4)$$

$$\Delta G° = \Delta H° - T\Delta S° \quad (5)$$

RESULTS AND DISCUSSION

Characterisation

Figure 3a displays the FTIR spectra from 4000 to 500 cm^{-1} of the lateritic soil while Figure 3b depicts the XRD pattern of laterite.

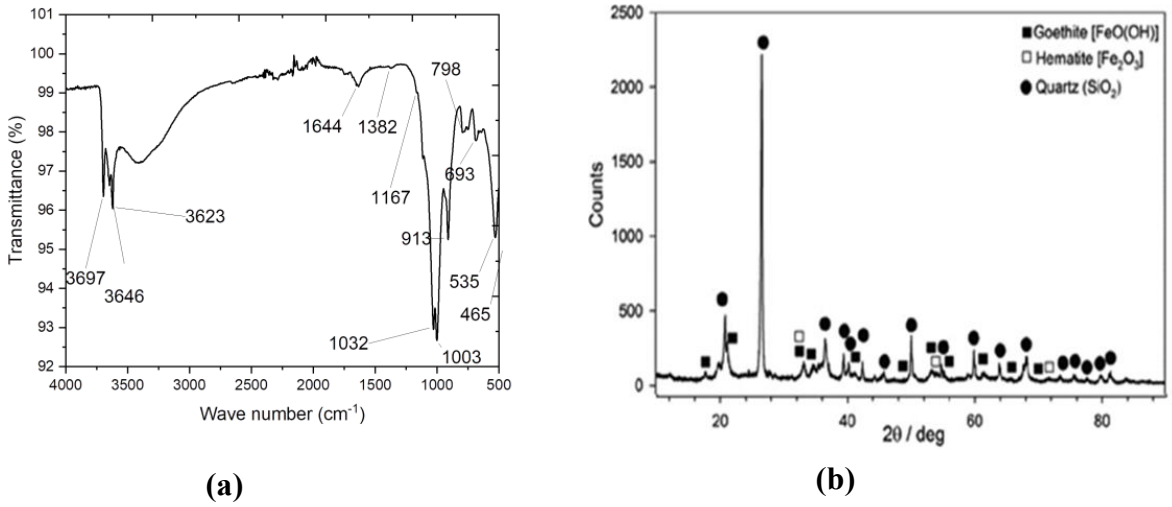

Fig. 3. (a): FTIR spectrum for laterite (b): Xray-diffraction patterns of laterite soil adsorbent

From Figure 3a, the band between 3697 and 3646 cm^{-1} was allocated to the –OH, Si, and Al groups. Water molecules were allocated to the 1644 cm^{-1} frequency band. The spectra showed bands at 1032, 1003, and 913 cm^{-1} due to the existence of Si–O–Fe, Al–OH, and Fe–OH vibrations, respectively. Laterite's hematite structure led to the Fe–O bonds extending at 535 cm^{-1} and 465 cm^{-1} of the spectra (Maiti et al., 2013). The most common phases were quartz (SiO_2), hematite (Fe_2O_3), and goethite ($FeO(OH)$) (Figure 3b). At extremely low intensity, several peaks suggested Al_2O_3. The laterite mineralogical phases utilised in this investigation are similar to laterite used in other studies (Forster et al., 2016).

Table 1 shows the band peaks and its respective chemical compounds found on the FTIR graph, whereas Table 2 gives the various percentages for the major oxides in the adsorbent.

Table 1: Classification of FTIR peaks

Wavenumber (cm^{-1})	Absorption range (cm^{-1})	Appearance	Group	Compound class
3697, 3646, 3623	3700 - 3584	Medium, Sharp	O-H stretching	Free alcohol
1644	1648 – 1638	Strong	C=C stretching	Monosubstituted alkene
1382	1385 – 1380	Medium	C-H bending	Gem dimethyl alkane
1167	1205 – 1124	Strong	C-O stretching	Secondary alcohol
1032	1070 – 1030	Strong	S=O stretching	Sulfoxide
913	915 – 905	Strong	C=C bending	Monosubstituted alkene
798	840 – 790	Medium	C=C bending	Trisubstituted alkene
693	730 – 665	Strong	C=C bending	Disubstituted (cis) alkene
535	600 – 500	Strong	C-I stretching	Halo compound

Table 2: Chemical constituents of laterite

Major Oxide	Value (%)
Al_2O_3	15.0
Fe_2O_3	40.1
SiO_2	33.2
MnO_2	0.7
P_2O_5	0.5
Na_2O_3	-
K_2O_3	0.8
CaO	-

Effect of Adsorbent Dosage on Removal Efficiency

The impact of laterite dosage on arsenic removal was investigated using varied masses of laterite adsorbent (1.0, 1.5, 2.0, 2.5, 3.0, and 3.5 mg) (Figure 4a). The removal efficiency for the optimum dosage, (3.5 mg) was determined by leaving it in contact with arsenic-contaminated water for 270 min and collecting a sample every 30 min (Figure 4b).

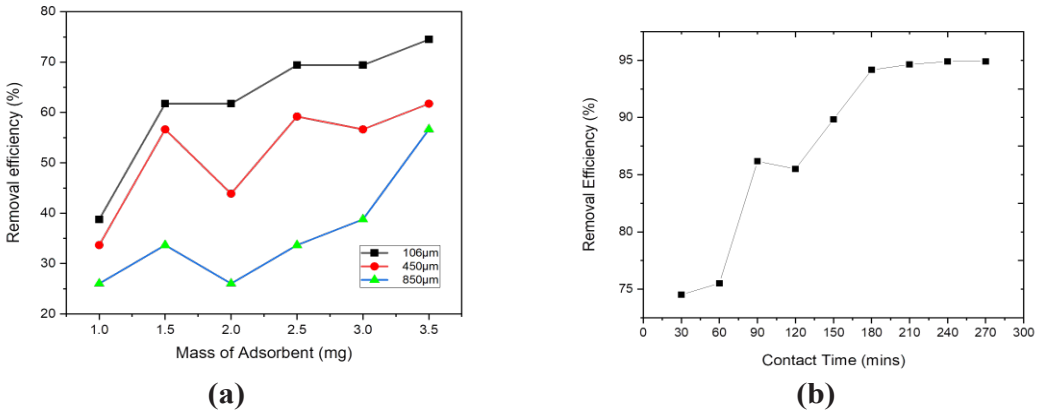

Fig. 4. (a) Effects of laterite dosage on arsenic removal efficiency
(b) Effect of contact time on adsorption of arsenic for optimum dosage

The concentration of the arsenic solution was kept constant at 0.0392 mg/L, while the volume was also kept constant at 100 mL. The removal effectiveness of the adsorbent rose with increasing adsorbent mass and with a decrease in particle size (Figure 4a). Thus, as the dosage of adsorbent increases, the removal efficiency increases, proving that the mass of adsorbent is directly proportional to removal efficiency (Mackenzie et al., 1979). Adsorption of arsenic from water proceeds in two stages: the first being a rapid formation of a monolayer, followed by a steady plateau sorption process (Mondal et al., 2008). This phenomenon explains the observation of rapid increase in the removal efficiency as the adsorbent dosage was gradually increased, followed by a steady rise in the removal efficiency until equilibrium was obtained. The number of active sites, surface area, and pores available for mass transfer also influenced the observation of higher removal efficiency as the dosage of adsorbent increased (Saadon et al., 2018). The effects of adsorbent dosage observed in this study are similar to those of other studies (Biltayib et al., 2021; Hassani et al., 2014; Padmavathy et al., 2016) that have reported that an increase in the adsorbent dosage over an optimum dose proceeds with a slow increase in the removal efficiency to a maximum value. Therefore, as the adsorbent dosage gets increased over the desired value, there is no significant impact on the sorption percentage of arsenic (Aryal et al., 2010). Increasing the adsorbent dosage over the optimum value also results in unsaturation of some binding sites, creating a limitation of arsenic mobility (Roy et al., 2013).

The change in contact time behaviour for a constant mass (the optimal dosage of 3.5 mg) is illustrated in Figure 4b. The removal efficiency recorded for the first 30 min was 74.52%. This increased up to the 90-min mark and it decreased for the next 30 minutes. The removal efficiency then increased steadily up to the 180-min mark at 94.90% and remained at equilibrium. This can be explained as follows: as adsorption process proceeds, the fixed adsorbent active sites get filled with the arsenic thereby decreasing the number of active sites available; at saturation point all the active sites get filled up and hence the rate of removal of arsenic stays at equilibrium (Mohammed et al., 2015). Similar observations are reported by other time-dependent adsorption research (Chen et al., 2011; Jiang et al., 2018; Zhang et al., 2013), presenting the most significant reason as the availability of empty internal and surface pores that get occupied by the adsorbate molecules as time progresses until reaching equilibrium (Olatunji et al., 2015). The removal effectiveness of arsenic by the laterite adsorbent improved with the increased contact time, according to the overall findings of the study.

Effect of Adsorbent Particle Size

As the mass of adsorbent increased with the varied particle sizes (106, 450, and 850 µm), the removal efficiency increased. The removal efficiency for 106 µm adsorbent size improved from 38.7 to 74.5%, while 450 µm particle size grew from 33.7 to 61.7%, and 850 µm particle size increased from 26 to 56% within the same time interval. The optimum removal effectiveness for the six masses employed in the adsorption tests occurred with 3.5 mg of the 106 µm laterite, with an average removal efficiency of 74.5% (Figure 4a). However, the removal efficiency increased to 94.90% at a contact time of 270 min (Figure 4b). Adsorbents with relatively smaller particle sizes have larger surface area. Coupled with the material's intrinsic properties of crystallinity and porosity, transport of adsorbates during the sorption process is facilitated. Particle size significantly affects the removal efficiency, as well as the adsorption capacity. The smaller the particle size, the faster the rate of adsorption, and hence the better the removal efficiency. In a study by Yusof *et al.* (2020), palm oil fuel ash (POFA) powder was used as adsorbent for removal of As(II) and As(V) from water, with a wide range of particle sizes between 30 and 125 µm. It was observed that when the smallest particle size of 30 µm was used, the maximum removal efficiency of 40 and 50% of As(II) and As(V) were obtained, respectively. Similarly, this observation is consistent with other studies (Huang et al., 2020; Kumar et al., 2019; Yi et al., 2020) which have reported that smaller particle sizes increase good contact between the adsorbate and the adsorbent, eventually increasing the removal efficiency and adsorption capacity (Aljeboree et al., 2017). The reduction in the removal efficiency as the particle size was increased in this study can therefore be attributed to the reduction in the surface area, thus fewer active sites on the laterite adsorbents to interact with the arsenic adsorbate.

Isotherm Modelling of Adsorption Data

Langmuir and Freundlich's isotherm models are utilised to explain the processes of arsenic ion adsorption onto laterite. Langmuir and Freundlich isotherm experiments were carried out to determine the maximum adsorption capacity of laterite adsorbent towards arsenic. The linearized form of the Langmuir isotherm model is provided in equation (1) with fitting plot shown in Figure 5a.

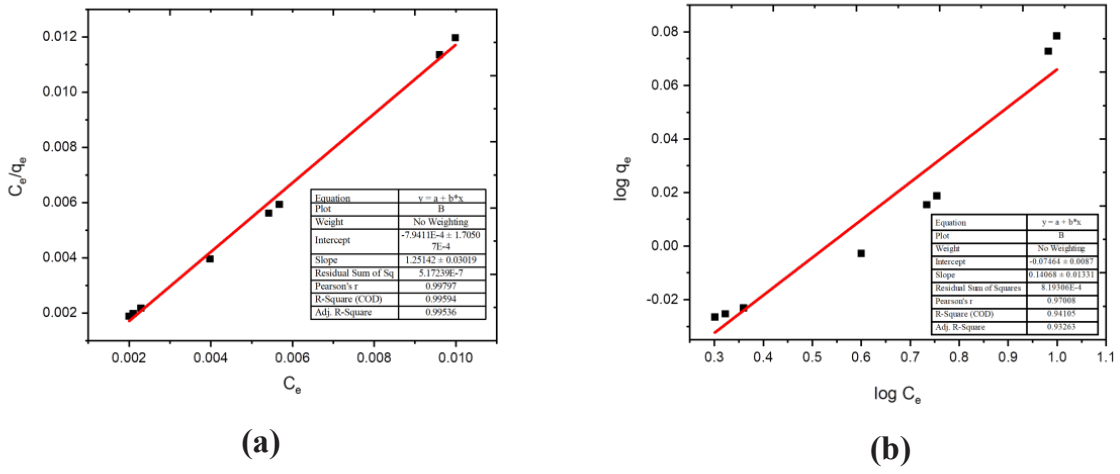

Fig. 5. (a) Langmuir Isotherm Model of the experimental data

(b) Freundlich Isotherm model fit of adsorption data

The adsorption constants of Langmuir isotherm model parameters, q_{max} and K_L, were estimated via the fitting plot from equation (1) and obtained as 0.799 mg/L and 1564.24 L/mg, respectively. The correlation coefficient of Langmuir isotherm (R^2) was 0.995 (Figure 5a), depicting a linear relationship between the plotted parameters (with R^2 value approximately 1). For an adsorption to obey the Langmuir isotherm model, a dimensionless factor, R_L must be satisfied. This factor is related to K_L and the initial concentration of adsorbate, C_o according to equation (6).

$$R_L = \frac{1}{1+K_L \times C_o} \quad (6)$$

The nature of adsorption is indicated by the value of R_L; for $R_L < 1$, adsorption is favorable; for >1, adsorption is unfavorable; for $R_L = 1$, adsorption is linear (Maji et al., 2008). The computed value of R_L from this study is 0.24, indicating a favorable adsorption. Thus, it was observed that the adsorption of arsenic onto laterite adsorbent correlated well with the Langmuir equation. Among the implications is that, metal ion absorption occurs on a homogeneous monolayer surface adsorption with no interaction between the adsorbed ions.

All surface sites are identical and can only accommodate one adsorbed molecule; a molecule's ability to be adsorbed on a given site is independent of its neighbouring site occupancy; adsorption is reversible, and the adsorbed molecule cannot migrate across the surface or interact with neighbouring molecules (Anah & Astrini, 2018).

The linear fit for the Freundlich model is shown in Figure 5b. According to equation (2), the Freundlich isotherm model parameters: adsorption capacity, K_F, and adsorption intensity index, n, are determined to be 0.842 and 7.107, respectively (Table 3). The correlation coefficient (R^2) for the Freundlich isotherm plot was 0.941 (Figure 5b). A summary of the Langmuir and Freundlich isotherm model parameters are presented in Table 3 from this study.

Table 3: Isotherm model parameters for Laterite adsorbent

Langmuir Adsorption Model				Freundlich Adsorption Model			
Adsorbent (mg)	K_L (L/mg)	q_{max} (mg/L)	R^2	Adsorbent Usage (mg)	K_F (L/mg)	n	R^2
3.5	1564.24	0.79911	0.9959	3.5	0.84217	7.10732	0.9411

Effect of Temperature on Arsenic adsorption

Figure 6 depicts the contact time behaviour at constant mass with temperature variation for the 106 μm adsorbent.

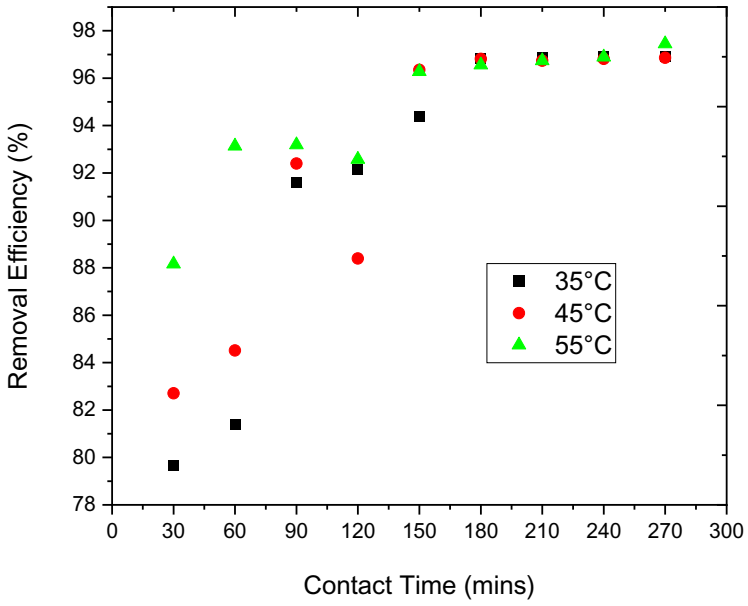

Fig. 6. Graph showing the effect of Temperature on adsorption

At a temperature of 35 °C and a constant mass of 3.5 mg for 30 min, the removal efficiency improves to 79.67% until it equilibrates at 96.94% roughly after 180 minutes. At a temperature of 45 °C and a constant mass of 3.5 mg, the removal effectiveness rises to 82.70% until it reaches 96.86% after 150 min of continuous arsenic adsorption. At a temperature of 55 °C and a constant mass of 3.5 mg, the removal efficiency rises from 88.16 to 97.45% after 180 min of continuous removal.

It was observed that when the temperature increased, the adsorbent's removal effectiveness improved. As the temperature rises, the mobility of ions or molecules in the flowing water accelerates, resulting in greater kinetic energy. As a result, the migration rate of arsenic ions onto the adsorbent's surface increased, increasing the adsorbent's adsorption capacity for arsenic ions. Other studies (Mohapatra et al., 2007) have shown, however, that a contrast observation in the removal efficiency is observed when the temperature is further increased. At higher temperatures, there is instability of the adsorbent-adsorbate complex, resulting in an escape of the adsorbed adsorbates from the adsorbent into the bulk solution. This unstable complex can also cause damage to the active sites of the adsorbents resulting in a decline in the adsorptive capacity and removal efficiency (Mohapatra et al., 2007).

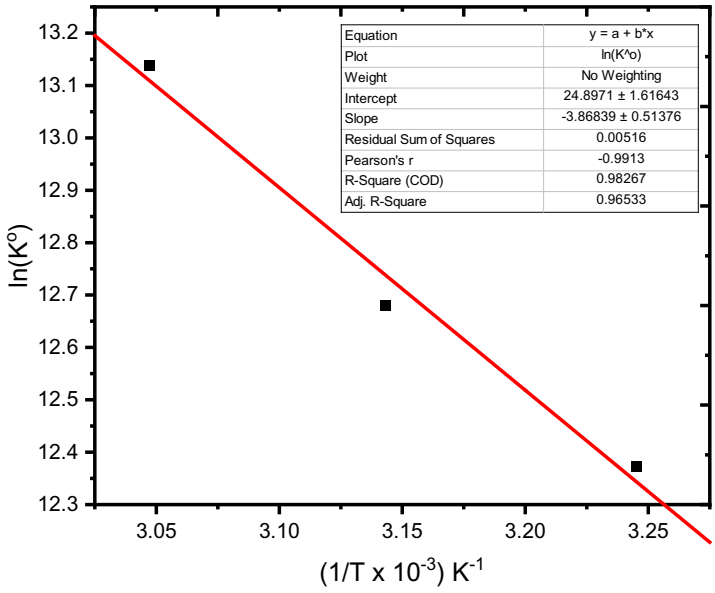

Fig. 7. Van't Hoff plot for thermodynamical studies

Thermodynamical Modelling

The Van't Hoff graph (Figure 7) which is a natural logarithm of K^o (log K^o) versus the reciprocal of the temperature ($^1/_T$) was first plotted. The thermodynamical parameters, enthalpy ($\Delta H°$) and entropy ($\Delta S°$) parameters were estimated from equations (3) and (4). The values of Gibb's free energy $\Delta G°$ (kJ/mol) were calculated from $\Delta H°$ and $\Delta S°$ (Table 4). The Van't Hoff plot indicates an endothermic adsorption process with the negative $\Delta G°$ values confirming the feasibility and spontaneity of the adsorption process.

Table 4: Thermodynamical Parameters for arsenic adsorption onto 106 µm Lateritic soil

Temperature T (K)	K_L (L/mg)	K_{L^o} (x 10^5)	In K_{L^o}	$\Delta G°$ (KJ/mol)	$\Delta H°$ (KJ/mol)	$\Delta S°$ (J/K mol)
308.15	3151.13	2.3608	12.37	-31.70	32.16	206.0
318.15	4285.60	3.2108	12.67	-33.54		
328.15	6785.01	5.0833	13.14	-35.85		

Conclusion and Recommendations

The goal of this study was to identify and synthesise low-cost adsorbents from locally available materials that have the potential to remove arsenic from water. The concentration of arsenic in river Ankobra was determined and batch adsorption adopted for the experiment. For the adsorption data, isotherm modelling, and effect of temperature were studied.

Laterite was prepared as an adsorbent for the removal of arsenic from polluted water in Ghana. Arsenic was removed from polluted water using the lateritic adsorbent at three different particles sizes. The laterite with the smallest particle size (106 μm) at a contact time of 270 min exhibited the best removal efficiency of 94.90 percent and the maximum adsorptive capacity of 1.063 mg/g. It was observed that as the temperature of the solution increased, adsorption is more efficient. The adsorption process was well-suited to the Langmuir isotherm model. The results indicate that metal ion absorption occurs on a homogenous surface via monolayer adsorption.

Further work would consider BET and SEM of the laterite sample. The determination of the surface area via BET and the phases via SEM of the particles will help explain the mechanism of the removal of arsenic by laterite. Additionally, composites with nanoparticles can be explored to enhance the removal efficiency of laterite. It is anticipated that these further works could produce a maximum adsorptive capacity for laterite that would compare with the 6.75 mg/g value obtained for red mud (Chakraborti et al., 2002).

Acknowledgement

The authors would like to acknowledge the insightful contributions from Associate Professor Emmanuel Nyankson and Mr. David Adebem Anafo of the Department of Materials Science and Engineering, University of Ghana. The contribution of Mr. Samuel Owusu-Atuah of the Department of Chemistry, University of Ghana, with the FTIR analysis is also duly acknowledged.

References

Aduah, M. S., Jewitt, G. P., & Toucher, M. L. (2018). Assessing impacts of land use changes on the hydrology of a lowland rainforest catchment in Ghana, West Africa. *Water, 10*(1), 9.

Aljeboree, A. M., Alshirifi, A. N., & Alkaim, A. F. (2017). Kinetics and equilibrium study for the adsorption of textile dyes on coconut shell activated carbon. *Arabian journal of chemistry, 10*, S3381-S3393.

Anah, L., & Astrini, N. (2018). Isotherm adsorption studies of Ni (II) ion removal from aqueous solutions by modified carboxymethyl cellulose hydrogel. IOP Conference Series: Earth and Environmental Science,

Anirudhan, T., & Unnithan, M. R. (2007). Arsenic (V) removal from aqueous solutions using an anion exchanger derived from coconut coir pith and its recovery. *Chemosphere, 66*(1), 60-66.

Aryal, M., Ziagova, M., & Liakopoulou-Kyriakides, M. (2010). Study on arsenic biosorption using Fe (III)-treated biomass of Staphylococcus xylosus. *Chemical Engineering Journal, 162*(1), 178-185.

Bagchi, S. (2007). Arsenic threat reaching global dimensions. In: Can Med Assoc.

Biltayib, B. M., Bonyani, M., Khan, A., Su, C.-H., & Yu, Y.-Y. (2021). Predictive modeling and simulation of wastewater treatment process using nano-based materials: Effect of pH and adsorbent dosage. *Journal of Molecular Liquids, 343*, 117611.

Brandhuber, P., & Amy, G. (2001). Arsenic removal by a charged ultrafiltration membrane—influences of membrane operating conditions and water quality on arsenic rejection. *Desalination, 140*(1), 1-14.

Chakraborti, D., Rahman, M. M., Paul, K., Chowdhury, U. K., Sengupta, M. K., Lodh, D., Chanda, C. R., Saha, K. C., & Mukherjee, S. C. (2002). Arsenic calamity in the Indian subcontinent: what lessons have been learned? *Talanta, 58*(1), 3-22.

Chen, S.-L., Dzeng, S. R., Yang, M.-H., Chiu, K.-H., Shieh, G.-M., Wai, C. M., & technology. (1994). Arsenic species in groundwaters of the blackfoot

disease area, Taiwan. *Environmental science*, *28*(5), 877-881.

Chen, Y.-G., Ye, W.-M., Yang, X.-M., Deng, F.-Y., & He, Y. J. E. E. S. (2011). Effect of contact time, pH, and ionic strength on Cd (II) adsorption from aqueous solution onto bentonite from Gaomiaozi, China. *Environmental Earth Sciences*, *64*(2), 329-336.

Chen, Y., & Zhang, D. (2014). Adsorption kinetics, isotherm and thermodynamics studies of flavones from Vaccinium Bracteatum Thunb leaves on NKA-2 resin. *Chemical Engineering Journal*, *254*, 579-585.

Choong, T. S., Chuah, T., Robiah, Y., Koay, F. G., & Azni, I. (2007). Arsenic toxicity, health hazards and removal techniques from water: an overview. *Desalination*, *217*(1-3), 139-166.

Forster, J., Pickles, C., & Elliott, R. J. M. E. (2016). Microwave carbothermic reduction roasting of a low grade nickeliferous silicate laterite ore. *88*, 18-27.

Hassani, A., Alidokht, L., Khataee, A., & Karaca, S. (2014). Optimization of comparative removal of two structurally different basic dyes using coal as a low-cost and available adsorbent. *Journal of the Taiwan Institute of Chemical Engineers*, *45*(4), 1597-1607.

He, J., & Charlet, L. (2013). A review of arsenic presence in China drinking water. *Journal of hydrology*, *492*, 79-88.

Huang, B., Yuan, Z., Li, D., Zheng, M., Nie, X., Liao, Y., & Impacts. (2020). Effects of soil particle size on the adsorption, distribution, and migration behaviors of heavy metal (loid) s in soil: a review. *Environmental Science: Processes*, *22*(8), 1596-1615.

Jiang, J., Li, W., Zhang, X., Liu, J., & Zhu, X. (2018). A new approach to controlling halogenated DBPs by GAC adsorption of aromatic intermediates from chlorine disinfection: effects of bromide and contact time. *Separation Purification Technology*, *203*, 260-267.

Kapaj, S., Peterson, H., Liber, K., & Bhattacharya, P. (2006). Human health effects from chronic arsenic poisoning–a review. *Journal of Environmental Science Health, Part A*, *41*(10), 2399-2428.

Karim, M. M. (2000). Arsenic in groundwater and health problems in Bangladesh. *Water Research*, *34*(1), 304-310.

Kumar, P. R., Chaudhari, S., Khilar, K. C., & Mahajan, S. P. (2004). Removal of arsenic from water by electrocoagulation. *Chemosphere*, *55*(9), 1245-1252.

Kumar, P. S., Korving, L., Keesman, K. J., van Loosdrecht, M. C., & Witkamp, G.-J. (2019). Effect of pore size distribution and particle size of porous metal oxides on phosphate adsorption capacity and kinetics. *Chemical Engineering Journal*, *358*, 160-169.

Mackenzie, F. T., Lantzy, R. J., & Paterson, V. (1979). Global trace metal cycles and predictions. *Journal of the International Association for Mathematical Geology*, *11*(2), 99-142.

Maiti, A., Thakur, B. K., Basu, J. K., & De, S. (2013). Comparison of treated laterite as arsenic adsorbent from different locations and performance of best filter under field conditions. *Journal of Hazardous materials*, *262*, 1176-1186.

Maji, S. K., Pal, A., & Pal, T. (2008). Arsenic removal from real-life groundwater by adsorption on laterite soil. *Journal of Hazardous materials*, *151*(2-3), 811-820.

Mandal, B. K., & Suzuki, K. T. (2002). Arsenic round the world: a review. *Talanta*, *58*(1), 201-235.

Matschullat, J. (2000). Arsenic in the geosphere—a review. *249*(1-3), 297-312.

Mohammed, J., Nasri, N. S., Zaini, M. A. A., Hamza, U. D., & Ani, F. N. (2015). Adsorption of benzene and toluene onto KOH activated coconut shell based carbon treated with NH3. *International Biodeterioration Biodegradation*, *102*, 245-255.

Mohapatra, D., Mishra, D., Chaudhury, G. R., & Das, R. P. (2007). Arsenic adsorption mechanism on clay minerals and its dependence on temperature. *Korean Journal of Chemical Engineering*, *24*(3), 426-430.

Mondal, P., Majumder, C., & Mohanty, B. (2008). Effects of adsorbent dose, its particle size and initial arsenic concentration on the removal of arsenic, iron and manganese from simulated ground water by Fe3+ impregnated activated carbon. *Journal of Hazardous materials*, *150*(3), 695-702.

Mostafa, M., & Hoinkis, J. (2012). Nanoparticle adsorbents for arsenic removal from drinking water: a review. *Journal of Environmental Science Health, Management Engineering Research*, *1*(1), 20-31.

Nagajyoti, P. C., Lee, K. D., & Sreekanth, T. (2010). Heavy metals, occurrence and toxicity for plants: a review. *Environmental chemistry letters*, *8*(3), 199-216.

Ning, R. Y. (2002). Arsenic removal by reverse osmosis. *Desalination*, *143*(3), 237-241.

Olatunji, M. A., Khandaker, M. U., Mahmud, H. E., & Amin, Y. M. (2015). Influence of adsorption parameters on cesium uptake from aqueous solutions-a brief review. *RSC advances*, *5*(88), 71658-71683.

Padmavathy, K., Madhu, G., & Haseena, P. (2016). A study on effects of pH, adsorbent dosage, time, initial concentration and adsorption isotherm study for the removal of hexavalent chromium (Cr (VI)) from wastewater by magnetite nanoparticles. *Procedia Technology*, *24*, 585-594.

Pierce, M. L., & Moore, C. B. (1982). Adsorption of arsenite and arsenate on amorphous iron hydroxide. *Water Research*, *16*(7), 1247-1253.

Roy, P., Mondal, N. K., Bhattacharya, S., Das, B., & Das, K. (2013). Removal of arsenic (III) and arsenic (V) on chemically modified low-cost adsorbent: batch and column operations. *Applied Water Science*, *3*(1), 293-309.

Saadon, S. A., Yunus, S. M., Yusoff, A. R., Yusop, Z., Azman, S., Uy, D., & Syafiuddin, A. (2018). Heated laterite as a low-cost adsorbent for arsenic removal from aqueous solution. *Malaysian Journal of Fundamental Applied Sciences*, *14*(1), 1-8.

Smedley, P. L., & Kinniburgh, D. G. (2002). A review of the source, behaviour and distribution of arsenic in natural waters. *Applied geochemistry*, *17*(5), 517-568.

Smith, A. H., & Smith, M. M. H. (2004). Arsenic drinking water regulations in developing countries with extensive exposure. *Toxicology*, *198*(1-3), 39-44.

Sorlini, S., & Gialdini, F. (2010). Conventional oxidation treatments for the removal of arsenic with chlorine dioxide, hypochlorite, potassium permanganate and monochloramine. *Water Research*, *44*(19), 5653-5659.

Viraraghavan, T., Subramanian, K., & Aruldoss, J. (1999). Arsenic in drinking water—problems and solutions. *Water Science and Technology*, *40*(2), 69-76.

Wang, S., & Mulligan, C. N. (2006). Occurrence of arsenic contamination in Canada: sources, behavior and distribution. *Science of the total Environment*, *366*(2-3), 701-721.

Yi, M., Cheng, Y., Wang, Z., Wang, C., Hu, B., & He, X. (2020). Effect of particle size and adsorption equilibrium time on pore structure characterization in low pressure N2 adsorption of coal: An experimental study. *Advanced Powder Technology*, *31*(10), 4275-4281.

Yusof, M. S. M., Othman, M. H. D., Wahab, R. A., Jumbri, K., Razak, F. I. A., Kurniawan, T. A., Samah, R. A., Mustafa, A., Rahman, M. A., & Jaafar, J. (2020). Arsenic adsorption mechanism on palm oil fuel ash (POFA) powder suspension. *Journal of Hazardous materials*, *383*, 121214.

Zhang, J., Cai, D., Zhang, G., Cai, C., Zhang, C., Qiu, G., Zheng, K., & Wu, Z. (2013). Adsorption of methylene blue from aqueous solution onto multiporous palygorskite modified by ion beam bombardment: Effect of contact time, temperature, pH and ionic strength. *Applied Clay Science*, *83*, 137-143.

INSTRUCTION FOR AUTHORS

SCOPE

Science and Development-the Journal of the College of Basic and Applied Sciences will publish original research articles, reviews and short communications in all scientific fields spanning agricultural, biological, engineering and physical sciences, with strong emphasis on promoting the link between science and development agenda. The journal aims to publish high quality articles rapidly and make these freely available to researchers world-wide through an open access policy.

Instructions to authors for submission of research article

Declarations/Acknowledgement

On submission, authors will be required to agree to the author's declaration confirming that:

- the work as submitted has not been published or accepted for publication, nor is being considered for publication elsewhere, either in whole or substantial part
- the work is original and all necessary acknowledgements have been made
- all authors have read the submitted version of the manuscript and approve its submission
- all persons entitled to authorship have been so included
- the authors must declare any conflict of interest
- the authors must state the contribution of each author in addition to a statement that each of the authors approved the manuscript before submission
- once a manuscript has been considered for publication, it cannot be withdrawn

Title page

The title page should:

- present a concise title that captures the essence of the work presented;
- list the full names, institutional addresses and email addresses for all authors (names of authors should be presented as e.g. Mercy Ama Opare and Justice Ofori Kuma Mintah)
- indicate the corresponding author and provide his/her email address

Abstract

The abstract should not exceed 300 words and should be one paragraph. The use of abbreviations should be minimized and do not cite references in the abstract. The abstract must provide context and purpose of the study, brief description of methods used and study area (where relevant), the main findings, brief summary and potential implications.

Keywords

Five to eight keywords representing the main content of the article

MAIN PAPER

Introduction

The introduction should explain the background to the study, its aims, a summary of the existing literature and why this study was necessary.

Methods

The methods section should include sampling, experimental design and setting of the study, a clear description of all analytical and experimental methods, processes, interventions and the type of statistical analysis used. Where proprietary brands are used in the research, include the brand names in parentheses.

Results

This should comprise the findings of the study, including, if appropriate, result of statistical analysis which must be included either in the text or as Tables and Figures.

Discussion

This section should discuss the implications of the findings in context of existing research and highlight limitations of the study. For study protocols and methodology manuscripts, this sections should include a discussion of any practical or operational issues involved in performing the study and any issues not covered in other sections.

Conclusions

This should state clearly the main conclusions and provide the explanation of the importance and relevance of the study to the field.

Ethics approval and consent to participate

Manuscripts reporting studies involving human participants, human data, human tissue or animals, must:

- include a statement on ethics approval (even where the need for approval was waived) and consent (in the case of human subjects)
- include the name of the ethics committee that approved the study and the committee's reference number if appropriate.

Sections heading

Sections should not be numbered. The subsections may be given a brief heading, with each heading appearing on a separate line.

Presentation

Font, Times New Roman, 12: double spacing, maximum of 15 pages (including references Figures and Tables). All "et als" must be italicized.

Referencing

The APA (American Psychological Association) referencing style must be used. For detailed information, please see the publication manual of the American Psychological Association, 6th edition, http://www.apastyle/org/ and http://blog.apastyle.org/ or the Taylor and Francis summary given here (http://www.tandf.co.uk/journals/authors/style/reference/tf_APA.pdf). References should be listed alphabetically and should not be numbered. See examples below

Book

Calfee, R. C., & Valencia, R. R. (1991). *APA guide to preparing manuscripts for journal publication.* Washington, DC: American Psychological Association.

Journal article

Kernis, M. H., Cornell, D. P., Sun, C. R., Berry, A., Harlow, T., & Bach, J. S. (1993). There's more to self-esteem than whether it is high or low: The importance of stability of self-esteem. *Journal of Personality and Social Psychology, 65,* 1190-1204.

Electronic source

Eco, U. (2015). How to write a thesis [PDF file]. (Farina C. M. & Farina F., Trans.) Retrieved from https://www.researchgate.net/...How_to_write_a_thesis/.../Umberto+Eco-How+to+Write+... (Original work published 1977).

Preparing figures

When preparing figures, please follow the formatting instructions below:

- Figures should be embedded in the main manuscript file (maximum five figures)
- All figures should be referred to in the text
- Each figure should be closely cropped to minimize the amount of white space surrounding the illustration
- Multi-panel figures (those with parts a, b, c, d etc.) should be labelled appropriately
- Figures should be numbered in the order they are first mentioned in the text, and uploaded in this order
- Figures should be in the correct orientation
- Figure titles (max. 15 words) and legends (max. 150 words) should be provided in the main manuscript
- Figure key should be incorporated into the graphic and not into the legend of the figure
- Individual figures should not exceed 10 MB. If a suitable format is chosen this file is adequate for extremely high quality figures.
- Please note that it is the responsibility of the author(s) to obtain permission from the copyright holder to reproduce figures (or tables) that have previously been published elsewhere. In order for all figures to be open access, authors must have permission from the rights holder if they wish to include images that have been published elsewhere in non-open access journals. Permission should be indicated in the figure legend, the original source included in the references list.

Figure file types

We accept the following file formats for figures:

- TIFF (suitable for images)
- JPEG (suitable for photographic images, less suitable for graphical images)
- PNG (suitable for images)
- BMP (suitable for images)
- CDX (ChemDraw- suitable for molecular structure)

Figure size and resolution

Figures are resized during publication detailed below:

Figures on the web:

- Width of 600 pixels (standard), 1200 pixels (high resolution)

Figures in the final PDF version:

- Width of 85 mm for half page width figure
- Width of 170 mm for full page width figure
- Maximum height of 225 mm for figure and legend.
- Image resolution of approximately 300 dpi (dots per inch) at the final size

Figures should be designed such that all information, including text, is legible at these dimensions. All lines should be wider than 0.25 pt when constrained to standard figure widths. All fonts must be embedded.

Preparing Tables

When preparing tables, please follow the formatting instructions below:

- Tables should be numbered and cited in the text in sequence using Arabic numerals (i.e. Table 1, Table 2 etc.)
- Table titles (max. 15 words) should be included above the table and legends (max. 150 words) should be included underneath the table
- Tables should not be embedded as figures or spreadsheet files, but should be formatted using 'Table object' function in your word processing program
- Tables should be included in the main manuscript file.
- Colour and shading may not be used in the tables. Parts of the table can be highlighted using superscript, numbering, lettering, symbols or bold text, the meaning of which should be explained in a table legend
- Commas should not be used to indicate numerical values

BIOLOGICAL & AGRICULTURAL SCIENCES

PHYSICAL & ENGINEERING SCIENCES

CBAS
College of Basic and Applied Sciences
University of Ghana

DigiBooks

ISSN 2550-3421